Numerical stability of coupling schemes in the 3d/0d modelling ofairflows and blood flows

Justine Fouchet-Incaux, Céline Grandmont, Sebastien Martin

NUMERICAL STABILITY OF COUPLING SCHEMES IN THE 3D/0D MODELLING OF AIRFLOWS AND BLOOD FLOWS

JUSTINE FOUCHET-INCAUX, CÉLINE GRANDMONT, AND SÉBASTIEN MARTIN

Abstract. We consider models which are classically used in the simulation of airflows and blood flows and investigate the numerical stability of some discretization strategies. The geometrical complexity of the networks in which air/blood flows leads to a classical decomposition of two areas: a truncated 3D geometry corresponding to the largest contribution of the domain and a 0D part connected to the 3D part, modelling air/blood flows in smaller airways/vessels. The resulting Navier-Stokes system in the 3D truncated part may involve non-local boundary conditions, deriving from a mechanical model. For various 3D/0D coupled models, different discretization processes are presented and analyzed in terms of numerical stability, highlighting strong differences according to the regimes that are considered. In particular, two main stability issues are investigated: first the coupling between the 3D and the 0D part for which implicit or explicit strategies are studied and, second, the question of estimating the amount of kinetic energy entering the 3D domain because of the artificial boundaries. In particular, we prove new estimates in appropriate norms for the discretized-in-time Navier-Stokes system. These estimates are derived under conditions on the smallness of the data, enlighting the intrinsic difficulty encountered with such systems to perform realistic simulations. We illustrate some of the theoretical results with numerical simulations, firstly in a single tube, then in a bifurcation geometry and finally in real geometries. Finally, we discuss the difference between airflows and blood flows in terms of numerical stability related to the magnitude of the physiological and physical parameters. Stokes and Navier-Stokes equations; coupling of models; numerical stability; numerical computations; finite element method.

1. Introduction

In the present work, we focus on the numerical simulation of physiological flows such as airflows in the respiratory tract, see e.g. [42, 2, 18, 30, 31, 26, 34] and blood flows in the arterial network, see e.g. [36, 41, 16, 13, 21, 35]. The underlying motivation is that simulations in patient-specific geometries may provide valuable informations to physicians to improve diagnosis, pulmonary drug delivery [29] or blood surgery [12]. In this context, direct simulations of 3D flows in such geometries are limited by the following constraints: since the whole respiratory tree and the blood network are very complex, with a lot of bifurcations, and with different scales therein, numerical costs related to a full 3D simulation in the whole domain are prohibitive. Not to mention that the image processing of the complete bronchial tree or blood network is out of reach for the time being. Therefore the whole domain is usually truncated, restricting the computational domain to a smaller part which is considered to be the most significant one in terms of flow description at the global scale: the large bronchi for airflows or the aorta region for blood flows. As a countereffect, the removed part has to be taken into account thanks to suitable reduced models in order to describe the global behaviour of the whole system.

Therein air and blood are commonly modelled as homogeneous, viscous, Newtonian and incompressible fluids. Thus we consider a system of partial differential equations involving the Navier-Stokes equations, which has to be coupled to reduced models to take into account phenomena in the removed part of the domain. In this work, we focus on *so-called* 0D models that describe how the fluid flux and average pressure on the artificial boundaries is related to the mechanical properties of the truncated part. The numerical analysis of such coupled systems is investigated, with special attention brought to applications related to airflows and blood flows modeling, which involve different kinds of 0D models sharing a similar formalism. The whole resulting system involves Navier-Stokes equations with nonlocal Neumann-type boundary conditions which depend on the chosen 0D model.

Many authors investigated the difficulties related to this kind of problems. From the theoretical point of view, one difficulty comes from the lack of energy estimate when considering the Navier-Stokes system with Neumann boundary conditions and more generally mixed Dirichlet-Neumann boundary conditions. Nevertheless existence of strong solutions (global in time for small data or local in time) has been shown in [25] under the assumption that the out/inlets meet the lateral boundary with a right angle and assuming some strong regularity results for the solution of the Stokes problem with mixed boundary conditions. Additionnally, when coupling the Navier-Stokes system with 0D reduced models, we refer to [38] and [20, 2] for the same type of existence results. In particular in [2] the regularity assumption that was previously mentioned has been dropped and the proof relies on the regularity results for the solution of the Stokes system, that have been derived in [32].

This paper is concerned with the numerical treatement of the coupled 3D/0D models arising in blood flows in large arteries as well as airflows in the bronchial tree. The efficiency of the numerical methods associated

Date: March 22, 2015.

to these problems relies on the analysis of two types of numerical difficulties: on the one hand, the explicit / implicit treatment of the nonlocal boundary conditions which couple the 3D and 0D models, which may lead to numerical instabilities and thus possible restrictions on the time-step, even with an implicit treatment of the coupling (when achieved by an iterative procedure). Note that in the targetted application fields the coupling strategies have been already implemented: the explicit treatment has been used for instance in hemodynamics in [41, 36]. Still in the context of hemodynamics the implicit coupling has been achieved by a Newton algorithm [13, 27] ; however, in each Newton sub-time-step, the coupling is explicit. The same strategy is used in [34] for mechanical ventilation in a rat bronchial tree. Moreover we refer for instance to [2] in the context of airflow modeling or [6] in the context of blood flows modeling where implicit monolithic coupling are considered. On the other hand, the more intrinsic difficulties coming from the convective term in the Navier-Stokes system which, as already stated, induces a lack of energy estimates and subsequent numerical instabilities. In particular it is well-known that, in practical simulations, when large pressure are applied, the system becomes unstable. To overcome this difficulty many strategies have been proposed: see [15] and [28] for a velocity profile constraining strategy or [4] and [21] for stabilization strategies, leading to the modification of the physical system (see [25] or more recently [17], [31] for reviews on these questions).

In Section 2, we present the physiological context and related 3D/0D models: Navier-Stokes equations with the *so-called* R model, RC model and RCR model. In Section 3, we focus on the numerical stability of the explicit / implicit treatment of the coupling and, consequently, we investigate the reduced 0D models together with the Stokes system, thus voluntarily omitting the nonlinear convective effects: we derive stability estimates in energy norms and pay a careful attention to the various physical parameters involved in these estimates to precisely quantify a possible CFL condition. In Section 4, we analyze the influence of the convective term in the Navier-Stokes system together with the 0D models: although energy estimates cannot be derived anymore, we obtain estimates in stronger norms as in the continuous framework. These new estimates are obtained for small data and only under the assumption that the out/inlets meet the lateral boundary with a right angle. As already mentionned, this illustrates the well-known difficulties encountered when performing simulations in a physiological context and the possible need to stabilize the numerical schemes. In Section 5, some of the theoretical results are illustrated by numerical simulations: computations, for the Stokes or the Navier-Stokes systems, are performed not only in idealized geometries (tube, bifurcation) but also in real geometries (truncated bronchial tree and blood network near the aorta) with parameters adapted to each application field.

2. Physiological flows in truncated domains

In this section, we describe two types of models associated to physiological flows: air through the bronchial tree and blood in the aorta network. The bronchial tree and the blood network have a complex structure which can be described as an assembly of tubes in which the biological fluid (air or blood) flows. For instance, the human respiratory tract is a dyadic tree of about 23 generations. The first generation (the trachea) has a length of about 10 centimetres, while the last one is about 1 millimeter. Until the 15th generation, the flow is convective whereas it is mainly diffusive in the acinar region. Moreover, the medical imaging techniques allow us to obtain a mesh only up to the 6th or 7th generation, see Figure 1-left. In the same way, the aorta network can be described as tube network.

In this context the complexity of the geometries makes it impossible to address direct simulations over the whole domain which then have to be truncated. Nevertheless, the removed parts corresponding to the smaller scales have to be taken into account in the global modelling: this can be done by defining appropriate reduced models. In the next subsections, we first describe the 3D part of the global model and, second, the reduced models which are classically used to mimick the fluid behaviour in the regions that have been truncated. Note that although the lung and the aorta lead to different types of 0D models, they share a similar formalism. In particular, this paper aims at understanding the possible differences between airflows and blood flows with respect to their numerical treatment.

2.1. Proximal part: three-dimensional geometries.

After truncation of the whole domain, we get a domain $\Omega \subset \mathbb{R}^3$ involving artificial boundaries, see Figure 1. We will note the inlet Γ_0 and the multiple outlets Γ_i, with $i \in \{1, \cdots, N_{\text{out}}\}$, N_{out} being the number of outlets. The lateral walls of the respiratory tree or of the aorta are noted Γ_ℓ.

In these 3D domains, we assume that the velocity $\mathbf{u}$ and the pressure p of the fluid satisfy the following incompressible Navier-Stokes system:

$$
\left\{
\begin{array}{rcll}
\rho(\partial_t \mathbf{u} + (\mathbf{u}\cdot\nabla)\mathbf{u}) - \eta\Delta\mathbf{u} + \nabla p &=& 0 & \text{in } \Omega, \\
\operatorname{div}(\mathbf{u}) &=& 0 & \text{in } \Omega, \\
\mathbf{u} &=& 0 & \text{on } \Gamma_\ell, \\
\eta\nabla\mathbf{u}\cdot\mathbf{n} - p\mathbf{n} &=& -p_0\mathbf{n} & \text{on } \Gamma_0, \\
\eta\nabla\mathbf{u}\cdot\mathbf{n} - p\mathbf{n} &=& -p_i\mathbf{n} & \text{on } \Gamma_i,\ i = 1, \ldots, N_{\text{out}}, \\
\mathbf{u}(0,\cdot) &=& \mathbf{u}_0 & \text{in } \Omega,
\end{array}
\right. \tag{1}
$$

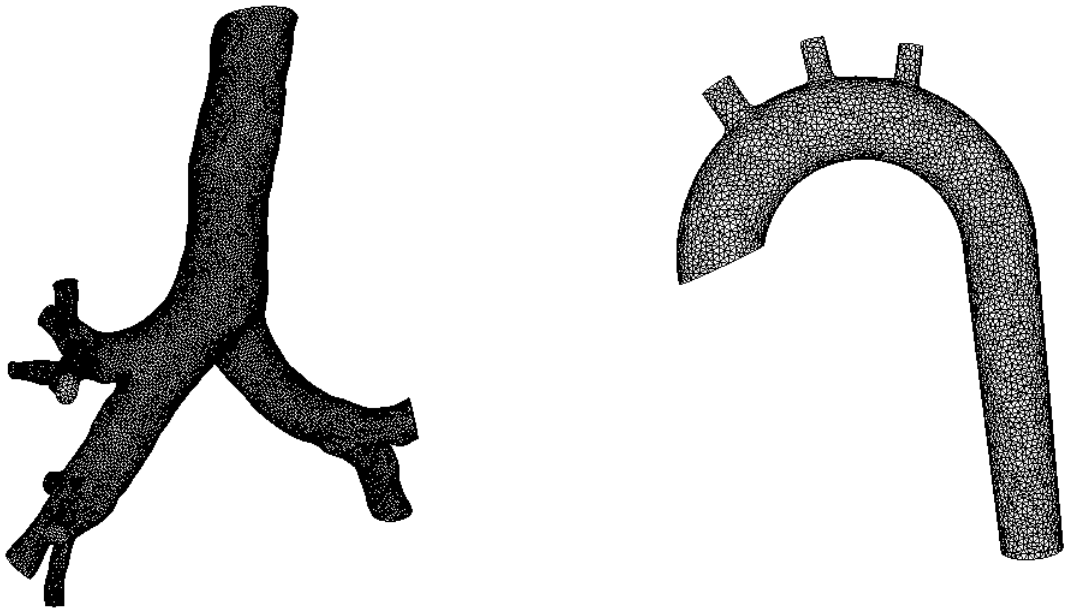

FIGURE 1. Real meshes of respiratory tract (left) and aorta (right).

with $\mathbf{u}_0$ the initial condition, $\mathbf{n}$ the outward unit vector on every part of the boundary $\partial\Omega$ and ρ and η the density and the viscosity of the fluid respectively. In order to model the whole system, i.e. the whole respiratory tree or the whole blood network, taking into account the fluid flow in the removed part, the 3D model has to be completed with a well-chosen reduced model. For instance, the removed part can be condensed into a 0D model (0D in the sense that it does not depend on a space variable) coupled to the 3D model at each outlet Γ_i. The interaction between the 3D and the 0D parts is taken into account by considering a generalized Neumann boundary conditions based upon the modelling of phenomena in the truncated part. Note that, as they involve the velocity flux at the artificial boundary, the boundary conditions are *nonlocal*:

$$p_i(t) = F_i(Q_i(s),\, 0 \le s \le t),$$

where Q_i is the flux on Γ_i. It depends on the instantaneous velocity field $\mathbf{u}$ at the boundary and is defined as

$$Q_i(s) = \int_{\Gamma_i} \mathbf{u}(s,\cdot)\cdot\mathbf{n}.$$

Function $F_i(\cdot)$ will be defined in next paragraphs, according to the considered application.

Remark 1. *In this work, several choice have been made:*

- *We express the Neumann condition by using the non-symmetric tensor* $\boldsymbol{\sigma} := \eta\nabla\mathbf{u} - p\,\mathbb{I}$. *This choice is more suitable from the physiological point of view when considering the truncation of cylindrical domains. An alternate choice could be based on the physical symmetric strain tensor* $\boldsymbol{\sigma}_{\text{symm.}} := \eta(\nabla\mathbf{u}+\nabla\mathbf{u}^{\mathrm{t}}) - p\,\mathbb{I}$ *and we refer to* [17] *for a comparison between the two versions.*
- *Lateral walls in the 3D part are assumed to be fully rigid and, consequently, we impose the fluid velocity to be equal to zero on* Γ_ℓ. *We refer to* [1, 19] *for more sophisticated models involving a deformable domain.*

2.2. **Distal part: truncation and related 0D models.** We introduce two different 0D models which describe the behaviour of the airflow or blood flow in the removed part. They involve different physiological parameters: the first one is the *resistance* of the truncated network. Indeed, assuming that the flow is laminar in the removed part, it can be characterized from Poiseuille law by a positive resistance parameter which depends on the fluid viscosity and the geometry of the domain ; the resistance of air or blood flows in a domain is due to the friction of fluid molecules with walls as the fluid flows through the geometry, which induces energy dissipation. The second major parameter involved in the 0D model is the *compliance* of the truncated network, which accounts for the elastic behaviour of the lung tissues or the deformable properties of the removed vessels.

Modelling of airflows: the RC model. Let us first focus on the airflow in the respiratory tract. As explained before, a 0D model is coupled at each ith artificial boundary of the three-dimensional geometry, see Figure 1-left. The coupling at the interfaces between 3D and 0D parts implies nonlocal Neumann boundary conditions illustrated by Figure 2 which uses an electrical analogy, see e.g. [34, 31]: The removed part is represented by its resistive and elastic global properties. Thus by two positive parameters R_i and C_i. For

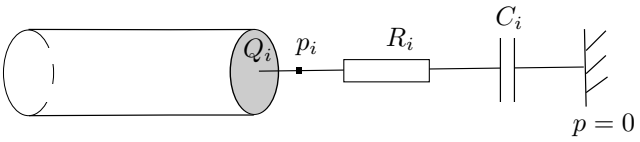

$$p_i(t) = R_i Q_i(t) + \frac{1}{C_i}\int_0^t Q_i(s)\,\mathrm{d}s$$

FIGURE 2. The RC reduced model.

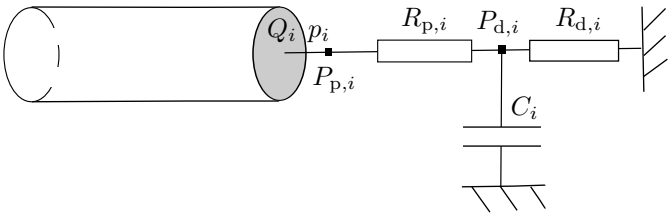

FIGURE 3. The RCR reduced model.

instance, when the lung is filled with air, it can restore the energy stored during the inspiration, without strain, like an elastic balloon that has been inflated. The elastic behaviour of the balloon is modeled by the compliance parameter C_i. As already mentionned the resistance parameter R_i models the resistance of the removed part to the fluid motion. Then

$$F_i(Q_i(s),\, 0 \le s \le t) = R_i Q_i(t) + \frac{1}{C_i}\int_0^t Q_i(s)\,\mathrm{d}s. \tag{2}$$

Note that the Neumann boundary value can be expressed as a function of the unknown velocity field $\mathbf{u}$:

$$F_i(Q_i(s),\, 0 \le s \le t) = R_i \int_{\Gamma_i} \mathbf{u}(t,\cdot)\cdot\mathbf{n} + \frac{1}{C_i}\int_0^t \int_{\Gamma_i} \mathbf{u}(s,\cdot)\cdot\mathbf{n}\,\mathrm{d}s.$$

Modelling of blood flows: the RCR model. Let us now focus on blood flows in the aortic region. A possible 0D model to describe the removed blood network involves two resistances and a compliance [33, 41, 36]. It leads to the RCR reduced model, see Figure 3.

This three-element model relates the pressure p_i $(= P_{\mathrm{p},i})$ and the flux Q_i on the outlet Γ_i through the following algebraic-differential equations (see, e.g., [16], Chapter 10):

$$\begin{cases} C_i \dfrac{\mathrm{d}P_{\mathrm{d},i}}{\mathrm{d}t} + \dfrac{P_{\mathrm{d},i}}{R_{\mathrm{d},i}} = Q_i, \\ P_{\mathrm{p},i} = R_{\mathrm{p},i} Q_i + P_{\mathrm{d},i}, \end{cases} \tag{3}$$

for $i = 1, ..., N_{\mathrm{out}}$. Solving the system (3), the general operator F_i in (1) can be defined as:

$$F_i(Q_i(s),\, 0 \le s \le t) = R_{\mathrm{p},i} Q_i(t) + P_{\mathrm{d},i}(0)\; e^{-t/\tau_i} + \frac{1}{C_i}\int_0^t Q_i(s) e^{(s-t)/\tau_i}\,\mathrm{d}s \tag{4}$$

where $\tau_i = R_{\mathrm{d},i} C_i$ denotes the characteristic time of relaxation of the reduced model. Here, $R_{\mathrm{p},i}$ and $R_{\mathrm{d},i}$ respectively model the proximal and distal vasculature, and the capacity C_i takes into account the deformable property of the downstream vessels. These three parameters are positive. The values $P_{\mathrm{p},i}$ and $P_{\mathrm{d},i}$ are respectively called proximal and distal pressures.

Regarding the existence of solutions for the Navier-Stokes system with mixed Dirichlet-Neumann boundary conditions, we refer to [25]: the authors prove the existence of a unique smooth solution which is local in time ; under an additional assumption on the smallness of the data, the smooth solution is proven to be global-in-time. Besides, the same type of result is obtained in [38] in which the authors studied the case of Robin-type boundary conditions which involves the modelling of a local-in-space resistive contribution: existence of a solution is obtained under the assumption that the resistance is small enough. In [2] a RC-like model is studied: the existence of a unique local-in-time strong solution for any data is proven; the particular case of a single R model is also investigated, leading to the existence and uniqueness of a global-in-time smooth solution for small data even if the resistance is large. Finally in [38], existence of a local-in-time strong solution for the RCR model (see Equations (1)-(3)) is proven for small data. Proofs of the above results are all based upon Galerkin approximations with special bases. Note moreover that they all require that in/outlet meet the lateral boundary with right angles. This framework will be used in the analysis of the semi-discretized Navier-Stokes systems, see Section 4. We point out that the main difficulty in the above references relies on the estimate of the convective term of the Navier-Stokes system. In what follows, before focusing on the influence of the convective term (in Section 4), we first focus on the Stokes system and the coupling strategies between the 3D and 0D models in Section 3.

3. Stokes system and reduced models

We investigate the numerical stability of various coupling strategies between the Stokes system and the 0D models that have been introduced in Section 2. In particular, we aim at deriving sharp energy estimates on the solution of the discretized-in-time or fully-discretized system and pay attention to the sensitivity of the stability constants or possible CFL conditions with respect to the parameters, either physiological ones (resistance R, compliance C, density ρ, viscosity η) or numerical ones (time-step Δt and mesh size h).

A secondary goal is to discuss the relative difficulties in simulating airflows and blood flows in physiological contexts. Indeed, models used for the respiratory system or for the blood network are not very different, and the way to deal with the involved nonlocal boundary conditions are also similar. However, applied pressures, physiological parameters and then flow regimes differ in terms of magnitude. Consequently, we will see that, according to the considered application, the numerical strategies may lead to different observations.

In what follows, discretized-in-time systems will be referred as semi-discretized systems, whereas fully-discretized systems will refer to systems that have been discretized both in time and space. Let $\Delta t > 0$ be the time step and $t^n = n\Delta t,\ n \in \{0, \dots, N\}$, with $N\Delta t = T$. We denote by $(\mathbf{u}^n, p^n)$ the approximated solution at time t^n of the continuous velocity and pressure fields $t \mapsto (\mathbf{u}(t,\cdot), p(t,\cdot))$. If we discretize in time the linear version of system (1), using the first order backward Euler scheme for the time derivative, the approximated velocity and pressure $\mathbf{u}^{n+1}$ and p^{n+1} satisfy:

$$
\left\{
\begin{array}{rcll}
\rho\dfrac{\mathbf{u}^{n+1}-\mathbf{u}^n}{\Delta t} - \eta\Delta\mathbf{u}^{n+1} + \nabla p^{n+1} &=& 0 & \text{in } \Omega,\\
\operatorname{div}(\mathbf{u}^{n+1}) &=& 0 & \text{in } \Omega,\\
\mathbf{u}^{n+1} &=& 0 & \text{on } \Gamma_\ell,\\
\eta\nabla\mathbf{u}^{n+1}\cdot\mathbf{n} - p^{n+1}\mathbf{n} &=& -p_0^{n+1}\mathbf{n} & \text{on } \Gamma_0,\\
\eta\nabla\mathbf{u}^{n+1}\cdot\mathbf{n} - p^{n+1}\mathbf{n} &=& F_{i,\Delta t}((Q_i^k)_{0\le k\le m}) & \text{on } \Gamma_i,\ i=1,...,N_{\text{out}},\\
\mathbf{u}^0 &=& \mathbf{u}_0 & \text{in } \Omega.
\end{array}
\right. \tag{5}
$$

Function $F_{i,\Delta t}$ is a time approximation of F_i with respect to the time-step Δt. It depends on the approximations $(Q_i^k)_{0\le k\le m}$ of the fluxes $(Q_i(t^k))_{0\le k\le m}$. Note that we may consider either explicit coupling with $m = n$ or implicit coupling with $m = n+1$. Let us now introduce the following useful functional spaces:

- $\mathbf{V} = \{\mathbf{v} \in \mathbf{H}^1(\Omega),\ \mathbf{v} = 0 \text{ on } \Gamma_\ell\}$,
- $\mathbf{V}_{\text{div}} = \{\mathbf{v} \in \mathbf{V},\ \operatorname{div}(\mathbf{v}) = 0\}$,
- $\mathbf{H} = \overline{\mathbf{V}_{\text{div}}}^{\mathbf{L}^2(\Omega)}$,
- $M = L^2(\Omega)$.

Note that, in particular, $\mathbf{V}$ a closed subspace of $\mathbf{H}^1(\Omega)$ such that $\mathbf{H}^1_0(\Omega) \subset \mathbf{V} \subset \mathbf{H}^1(\Omega)$. We denote by $(\cdot,\cdot)_\Omega$ the $L^2(\Omega)$-inner product and by $\|\cdot\|_{L^2(\Omega)}$ the $L^2(\Omega)$-norm. In what follows, $\tilde{c}$ stands for a generic positive constant whose value may change between lines, and which only depends on the geometry of the problem: $\tilde{c} = \tilde{c}(\Omega)$. In particular it does not depend on physical or discretization parameters. We also recall the following lemma which will be extensively used in the analysis of the problem:

Lemma 1. *There exists $\tilde{c} > 0$ such that, for any $i = 0, ..., N_{\text{out}}$,*

$$\left|\int_{\Gamma_i} \mathbf{v}\cdot\mathbf{n}\right| \le \tilde{c}\|\mathbf{v}\|_{L^2(\Omega)},\ \forall \mathbf{v} \in \mathbf{H}.$$

We refer the reader to [2] for the proof of this lemma. Note that this estimate is deeply based on the divergence-free property and on the fact that $\overline{\Gamma_i} \cup \overline{\Gamma_j} = \emptyset$ for all $i \neq j$.

Without loss of generality, the stability analysis may be led in a 3D domain with only *one single outlet*, i.e. $N_{\text{out}} = 1$. This is the reason why we will deal with a 3D system only coupled to a one-element nonlocal boundary condition in Sections 3 and 4, in which case subscripts i will be voluntarily omitted.

3.1. R model.

Let us first consider the Stokes system coupled to a resistance reduced model. It consists in considering the following approximation:

$$F_{\Delta t}((Q^k)_{0\le k\le m})) = \left\{
\begin{array}{ll}
RQ^n & \text{in the explicit coupling,}\\
RQ^{n+1} & \text{in the implicit coupling.}
\end{array}
\right.$$

The variational formulation associated to the explicit coupling between the Stokes system and the 0D model can be written as follows:

Scheme 1 (Semi-discretized Stokes problem with explicit coupling)**.** *Let* $\mathbf{u}^0 = \mathbf{u}_0 \in \mathbf{V}_{\mathrm{div}}$ *be the initial data, find* $(\mathbf{u}^{n+1}, p^{n+1})$ *in* $\mathbf{V} \times M$ *such that, for all* $(\mathbf{v}, q) \in \mathbf{V} \times M$*,*

$$\begin{aligned} \frac{\rho}{\Delta t}\int_\Omega \mathbf{u}^{n+1}\cdot\mathbf{v} + \eta\int_\Omega \nabla\mathbf{u}^{n+1} : \nabla\mathbf{v} + \int_\Omega q\mathrm{div}(\mathbf{u}^{n+1}) + \int_\Omega p^{n+1}\mathrm{div}(\mathbf{v}) \\ = \frac{\rho}{\Delta t}\int_\Omega \mathbf{u}^{n}\cdot\mathbf{v} - \int_{\Gamma_0} p_0^{n+1}\mathbf{v}\cdot\mathbf{n} - R\left(\int_{\Gamma_1}\mathbf{u}^n\cdot\mathbf{n}\right)\left(\int_{\Gamma_1}\mathbf{v}\cdot\mathbf{n}\right). \end{aligned} \tag{6}$$

The explicit treatment has been already used in hemodynamics, see e.g. [41, 36]. Dealing with the implicit treatment, the variational formulation associated to the coupling between the Stokes system and the 0D model can be written as follows:

Scheme 2 (Semi-discretized Stokes problem with implicit coupling)**.** *Let* $\mathbf{u}^0 = \mathbf{u}_0 \in \mathbf{V}_{\mathrm{div}}$ *be the initial data, find* $(\mathbf{u}^{n+1}, p^{n+1})$ *in* $\mathbf{V} \times M$ *such that, for all* $(\mathbf{v}, q) \in \mathbf{V} \times M$*,*

$$\begin{aligned} \frac{\rho}{\Delta t}\int_\Omega \mathbf{u}^{n+1}\cdot\mathbf{v} + \eta\int_\Omega \nabla\mathbf{u}^{n+1} : \nabla\mathbf{v} + \int_\Omega q\mathrm{div}(\mathbf{u}^{n+1}) + \int_\Omega p^{n+1}\mathrm{div}(\mathbf{v}) \\ + R\left(\int_{\Gamma_1}\mathbf{u}^{n+1}\cdot\mathbf{n}\right)\left(\int_{\Gamma_1}\mathbf{v}\cdot\mathbf{n}\right) = \frac{\rho}{\Delta t}\int_\Omega \mathbf{u}^{n}\cdot\mathbf{v} - \int_{\Gamma_0} p_0^{n+1}\mathbf{v}\cdot\mathbf{n}. \end{aligned} \tag{7}$$

Considering an implicit coupling modifies the bilinear form of the variational problem. Indeed, it now contains a product of integrals, namely the bilinear term

$$R\left(\int_{\Gamma_1}\mathbf{u}^{n+1}\cdot\mathbf{n}\right)\left(\int_{\Gamma_1}\mathbf{v}\cdot\mathbf{n}\right)$$

in Eq. (7). Then, in a finite element framework, the pattern of the rigidity matrix is modified and filled: the matrix elements associated to the nodes at the 3D-0D interface are non-zero. We can directly assemble the new terms, modifying the pattern of the matrix. This is the method used in Section 5 for the computations. Note that it is possible to avoid the assembling of the rigidity matrix by using an iterative method that only requires matrix-vector products. Another way to treat the implicit coupling is to consider the algorithm introduced in [10, 31]. This method only uses elementary solutions of the classical Stokes problem with standard boundary conditions (Dirichlet and Neumann). Then the strategy relies on the linear nature of the problem, the implicit boundary condition being imposed thanks to a suitable combination of the elementary solutions. Note that, when considering the Navier-Stokes system, this strategy can be generalized if the convective term is discretized with a suitable method such as the characteristics method. Furtherthemore, in [13, 27], the authors develop a solver for Scheme 2 using a Newton algorithm. However, in each Newton sub-time-step, the coupling is explicit. Then each Newton sub-iteration inherits the properties of the explicit coupling (possible drawbacks included).

Before entering into details of the numerical analysis, let us present some preliminary computations that reveal possible instabilities of the considered schemes. The first step consists in computing the solution of Scheme 1 and observe the stability of the solution. In Figure 4, we impose a sinusoidal pressure at the inlet and we plot the flux of the solution at the outlet. We observe that the behaviour of the numerical solution depends on the time-step: numerical instabilities (Figure 4(a)), numerical oscillations (Figure 4(b)), stable and non-oscillatory behaviour (Figure 4(c)) when the time-step is sufficiently small. If the implicit coupling is used, the numerical solution is unconditionnally stable (Figure 4(d)).

Note that another source of instabilities comes from the Neumann boundary condition at the inlet, together with the convective term of the Navier-Stokes equations. Indeed, in Figure 4, we compare the flux of the solution at the inlet for Stokes or Navier-Stokes system, for different time-steps. Figures 4(e) and 4(f) illustrate that even with an implicit treatment, instabilities may appear, and this occurs even with a very small time-step. This point will be further discussed in Section 4 (and Subsection 5.4 for numerical simulations).

Let us now analyze the numerical stability of Problems 2 and 1 by deriving discrete energy estimates. Let us begin with the implicit scheme.

Theorem 1 (Implicit coupling for the R model)**.** *The approximation of the velocity provided by the implicit coupling scheme (see Eq.* (7) *in Scheme 2) is unconditionally stable and its energy is bounded:*

$$\frac{\rho}{2}\|\mathbf{u}^n\|^2_{L^2(\Omega)} + \frac{\eta}{2}\sum_{k=1}^n \Delta t\|\nabla\mathbf{u}^k\|^2_{L^2(\Omega)} + R\sum_{k=1}^n \Delta t\left(\int_{\Gamma_1}\mathbf{u}^k\cdot\mathbf{n}\right)^2 \le \frac{\rho}{2}\|\mathbf{u}^0\|^2_{L^2(\Omega)} + \frac{\tilde{c}}{\eta}\sum_{k=1}^n \Delta t\|p_0^k\|^2_{L^2(\Omega)},$$

for all $n \in \{1, ..., N\}$.

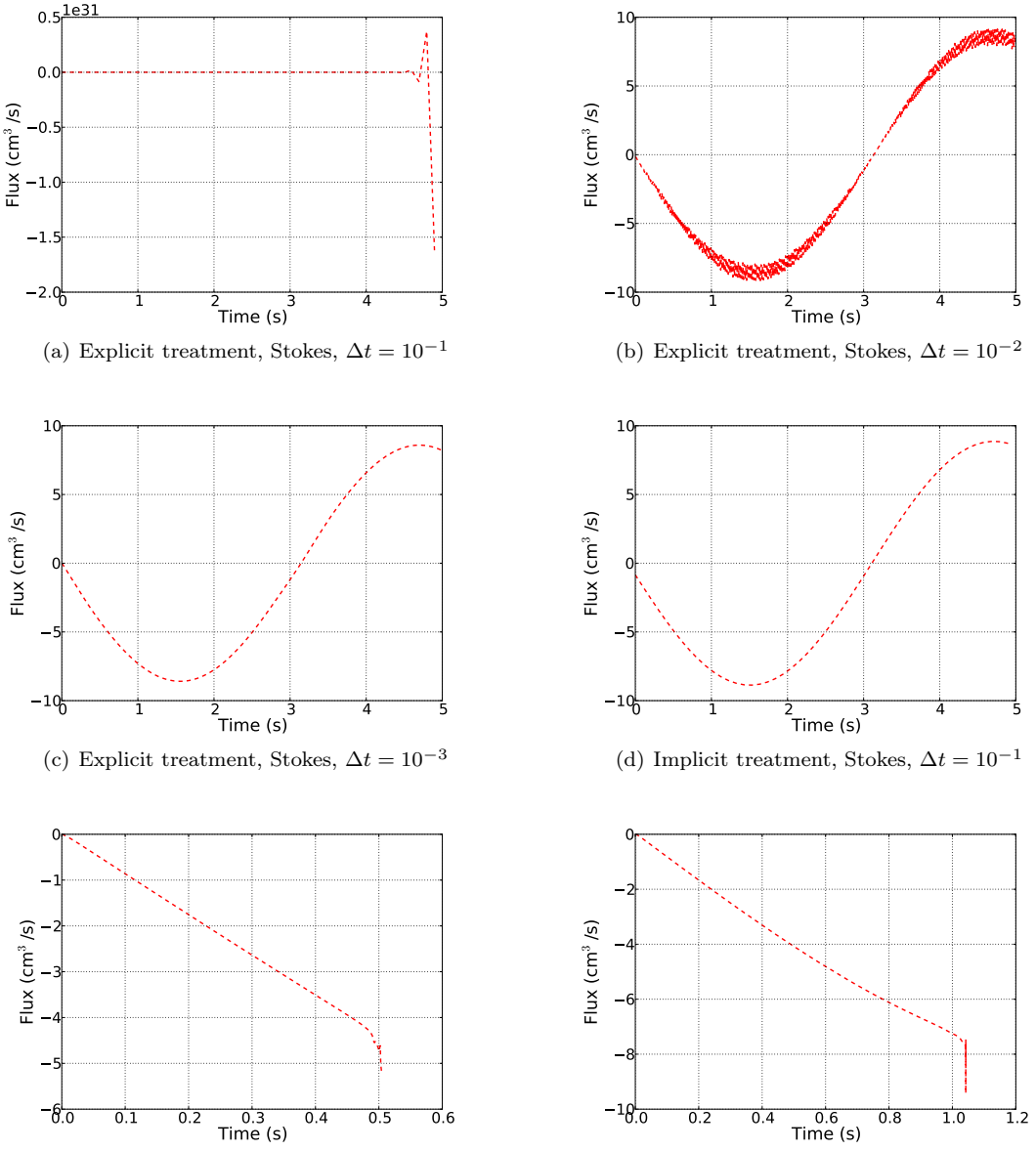

(a) Explicit treatment, Stokes, $\Delta t = 10^{-1}$

(b) Explicit treatment, Stokes, $\Delta t = 10^{-2}$

(c) Explicit treatment, Stokes, $\Delta t = 10^{-3}$

(d) Implicit treatment, Stokes, $\Delta t = 10^{-1}$

(e) Implicit treatment, Navier-Stokes, $\Delta t = 10^{-3}$

(f) Implicit treatment, Navier-Stokes, $\Delta t = 10^{-5}$

FIGURE 4. Flux at the inlet, single tube with $p_0^{n+1}(t) = 100 \cdot \sin(t^{n+1})$ and $R = 10$. CGS units.

Proof. Taking $\mathbf{v} = \mathbf{u}^{n+1}$ as a test function in the variational formulation associated to Scheme 2 and multipling by Δt, we obtain:

$$\begin{aligned} &\frac{\rho}{2}\|\mathbf{u}^{n+1}\|^2_{L^2(\Omega)} - \frac{\rho}{2}\|\mathbf{u}^{n}\|^2_{L^2(\Omega)} + \frac{\rho}{2}\|\mathbf{u}^{n+1} - \mathbf{u}^{n}\|^2_{L^2(\Omega)} \\ &+ \eta\Delta t\|\nabla\mathbf{u}^{n+1}\|^2_{L^2(\Omega)} + R\Delta t\left(\int_{\Gamma_1}\mathbf{u}^{n+1}\cdot\mathbf{n}\right)^2 + \Delta t\int_{\Gamma_0} p_0^{n+1}\mathbf{u}^{n+1}\cdot\mathbf{n} = 0. \end{aligned} \tag{8}$$

We observe three kinds of dissipations: a numerical dissipation from the Euler scheme ($\frac{\rho}{2}\|\mathbf{u}^{n+1} - \mathbf{u}^{n}\|^2_{L^2(\Omega)}$), and two physical dissipations related to the viscosity of the fluid: the viscous dissipation in the 3D part

$$\eta\Delta t\|\nabla\mathbf{u}^{n+1}\|^2_{L^2(\Omega)},$$

and the viscous dissipation of the 0D part

$$R\Delta t\left(\int_{\Gamma_1}\mathbf{u}^{n+1}\cdot\mathbf{n}\right)^2.$$

This last term is positive, that will ensure the unconditional stability of the implicit scheme. Using a trace inequality and Young inequality, the term $\Delta t \int_{\Gamma_0} p_0^{n+1}\mathbf{u}^{n+1}\cdot\mathbf{n}$ can be controlled by:

$$\left|\Delta t \int_{\Gamma_0} p_0^{n+1}\mathbf{u}^{n+1}\cdot\mathbf{n}\right| \leq \frac{\eta\Delta t}{2}\|\nabla\mathbf{u}^{n+1}\|^2_{L^2(\Omega)} + \frac{\tilde{c}\Delta t}{2\eta}\|p_0^{n+1}\|^2_{L^2(\Gamma_0)}. \tag{9}$$

We now proceed by inserting (9) into (8), and by summation. Noting that $\frac{\rho}{2}\|\mathbf{u}^{n+1}-\mathbf{u}^n\|^2_{L^2(\Omega)} \geq 0$, the result holds and the velocity approximation belongs to the discrete energy spaces. □

Remark 2. *According to the application, the amplitude of the applied pressures may differ a lot. Consequently, so does the energy bound. Moreover the estimate* (9) *is not satisfactory when* η *tends to* 0*. However, if* p_0^{n+1} *is constant in space on* Γ_0*, the power associated to the inlet pressure can be controlled using Lemma 1 and Young inequality:*

$$\begin{aligned}\left|\Delta t \int_{\Gamma_0} p_0^{n+1}\mathbf{u}^{n+1}\cdot\mathbf{n}\right| &\leq \Delta t|p_0^{n+1}|\ \left|\int_{\Gamma_0}\mathbf{u}^{n+1}\cdot\mathbf{n}\right|,\\ &\leq \tilde{c}\Delta t|p_0^{n+1}|\|\mathbf{u}^{n+1}\|_{L^2(\Omega)},\\ &\leq \frac{\tilde{c}\Delta t}{4\rho}|p_0^{n+1}|^2 + \Delta t\frac{\rho}{4}\|\mathbf{u}^{n+1}\|^2_{L^2(\Omega)}.\end{aligned}$$

Consequently if the time step Δt *is small enough, the last term of the previous inequality can be absorbed by the term* $\frac{\rho}{2}\|\mathbf{u}^{n+1}\|^2_{L^2(\Omega)}$ *on the left hand side of the energy inequality. Thus, by a discrete Gronwall lemma, we obtain again that the velocity approximation belongs to the discrete energy spaces, but with an additional exponential growth (*$e^{\rho\tilde{c}T}$*) on the right-hand-side of the estimate and under a CFL condition.*

Let us now focus on the explicit treatment which has been used in blood flow framework, for instance in [41, 36]. In particular, we derived discrete energy estimates addressing the numerical stability of the scheme.

Theorem 2 (Explicit coupling for the R model)**.** *The approximation of the velocity provided by the implicit coupling scheme (see Eq.* (6) *in Scheme 1) satisfies the following estimates:*

- *Result 1: the following discrete energy estimate holds:*

$$\frac{\rho}{2}\|\mathbf{u}^n\|^2_{L^2(\Omega)} + \frac{\eta}{4}\sum_{k=1}^{n}\Delta t\|\nabla\mathbf{u}^k\|^2_{L^2(\Omega)} \leq \left(\frac{\tilde{c}}{\eta}\sum_{k=1}^{n}\Delta t\|p_0^k\|^2_{L^2(\Gamma_0)} + \frac{\rho}{2}\|\mathbf{u}^0\|^2_{L^2(\Omega)}\right)\exp\left(\frac{\tilde{c}R^2T}{\eta}\right),$$

  for all $n\in\{1,...,N\}$*.*
- *Result 2: Under the condition*

$$\eta \geq \widetilde{c}R, \tag{10}$$

  the following discrete energy inequality holds:

$$\frac{\rho}{2}\|\mathbf{u}^n\|^2_{L^2(\Omega)} + \frac{\eta\Delta t}{4}\|\nabla\mathbf{u}^n\|^2_{L^2(\Omega)} \leq \frac{\tilde{c}}{\eta}\sum_{k=1}^{n}\Delta t\|p_0^k\|^2_{L^2(\Gamma_0)} + \frac{\rho}{2}\|\mathbf{u}^0\|^2_{L^2(\Omega)} + \frac{\eta\Delta t}{4}\|\nabla\mathbf{u}^0\|^2_{L^2(\Omega)}.$$

  for all $n\in\{1,...,N\}$*.*
- *Result 3: If the time-step satisfies the following condition:*

$$\Delta t \leq \widetilde{c}\frac{\rho}{R}, \tag{11}$$

  then, defining $\gamma = 1-\frac{\tilde{c}R\Delta t}{\rho}$*, the following estimate holds*

$$\frac{\rho}{2}\|\mathbf{u}^n\|^2_{L^2(\Omega)} + \frac{\eta}{2}\sum_{k=1}^{n}\Delta t\|\nabla\mathbf{u}^k\|^2_{L^2(\Omega)} \leq \left(\frac{\tilde{c}}{\eta}\sum_{k=1}^{n}\Delta t\|p_0^k\|^2_{L^2(\Gamma_0)} + \frac{\rho}{2}\|\mathbf{u}^0\|^2_{L^2(\Omega)}\right)\exp\left(\frac{\tilde{c}RT}{\gamma}\right),$$

  for all $n\in\{1,...,N\}$*.*

Remark 3 (Comments on Theorem 2)**.** *Since, considering a Poiseuille law,* R *is proportional to* η*, condition* (10) *is in fact a geometric condition, which will be satisfied or not according to the considered test-case. This kind of conditions also appears in* [38]*, where the authors study the existence of solutions for a similar system in the continuous framework. Note that in* Result 2 *which is obtained under condition* (10)*, no bound for the discrete energy dissipation of the fluid (i. e.* $\sum_{k=1}^{n}\Delta t\|\nabla\mathbf{u}^k\|^2_{L^2(\Omega)}$*) has been obtained. We only bound* $\Delta t\|\nabla\mathbf{u}^n\|^2_{L^2(\Omega)}$ *and furthermore we need the initial velocity* $\mathbf{u}^0$ *to be not only in* $\mathbf{L}^2(\Omega)$ *but also in* $\mathbf{H}^1(\Omega)$*. In the other two results, namely* Results 1 *and* 3*, we obtain a bound of the discrete dissipation energy of the fluid velocity with an upper bound involving an exponential growth. Note moreover that when condition* (10) *is not satisfied, if one wants to guarantee a bound that behaves like* $\exp(\tilde{c}RT)$*, which is better than* $\exp(\tilde{c}\frac{R^2T}{\eta})$ *since* $\eta<\tilde{c}R$*, it is enough to constrain the time-step so that condition* (11) *is satisfied.*

Remark 4. *Note that the order of magnitude of the CFL condition* (11) *depends on the considered application. Indeed the upper bound is propotional to ρ/R and thus to ρ/η which is nearly a hundred times larger in blood flows than in airflows.*

Proof. Considering the explicit coupling scheme, by taking $\mathbf{u}^{n+1}$ as a test function in Scheme 1, we obtain:

$$\begin{aligned}&\frac{\rho}{2}\|\mathbf{u}^{n+1}\|^2_{L^2(\Omega)} - \frac{\rho}{2}\|\mathbf{u}^{n}\|^2_{L^2(\Omega)} + \frac{\rho}{2}\|\mathbf{u}^{n+1}-\mathbf{u}^{n}\|^2_{L^2(\Omega)}\\ &+ \frac{\eta\Delta t}{2}\|\nabla\mathbf{u}^{n+1}\|^2_{L^2(\Omega)} + R\Delta t\left(\int_{\Gamma_1}\mathbf{u}^{n+1}\cdot\mathbf{n}\right)\left(\int_{\Gamma_1}\mathbf{u}^{n}\cdot\mathbf{n}\right) \leq \frac{\tilde{c}\Delta t}{2\eta}\|p_0^{n+1}\|^2_{L^2(\Gamma_0)}.\end{aligned} \tag{12}$$

The main point is to estimate $R\Delta t(\int_{\Gamma_1}\mathbf{u}^{n+1}\cdot\mathbf{n})(\int_{\Gamma_1}\mathbf{u}^{n}\cdot\mathbf{n})$ whose sign is not known. We will study the behaviour of the solution if neither (10) nor (11) are assumed to hold true (see *Result 1*). Then we will show that the energy of the approximation is bounded with a better upper bound if condition (10) is satisfied (see *Result 2*). To finish with, we show in *Result 3* that if condition (10) is not satisfied, one can get a better bound than in *Result 1* by choosing a time-step such that condition (11) is satisfied.

Proof of Result 1:

Firstly, we study the behaviour of the solution in a general case, considering that neither (10) nor (11) are necessarily satisfied. To deal with the product of integrals, we use Lemma 1 (since $\mathrm{div}(\mathbf{u}^n)=0$ for all n), a trace inequality and then Young inequality:

$$\begin{aligned}\left|R\Delta t\left(\int_{\Gamma_1}\mathbf{u}^{n+1}\cdot\mathbf{n}\right)\left(\int_{\Gamma_1}\mathbf{u}^{n}\cdot\mathbf{n}\right)\right| &\leq R\tilde{c}\Delta t\|\nabla\mathbf{u}^{n+1}\|_{L^2(\Omega)}\|\mathbf{u}^n\|_{L^2(\Omega)},\\ &\leq \frac{\eta\Delta t}{4}\|\nabla\mathbf{u}^{n+1}\|^2_{L^2(\Omega)} + \frac{R^2\tilde{c}\Delta t}{\eta}\|\mathbf{u}^n\|^2_{L^2(\Omega)},\end{aligned}$$

where $\frac{\eta\Delta t}{4}\|\nabla\mathbf{u}^{n+1}\|^2_{L^2(\Omega)}$ can be absorbed by the fluid dissipation on the left-hand side of (12). This yields the following estimate:

$$\frac{\rho}{2}\|\mathbf{u}^{n+1}\|^2_{L^2(\Omega)} + \frac{\eta}{4}\Delta t\|\nabla\mathbf{u}^{n+1}\|^2_{L^2(\Omega)} \leq \frac{\tilde{c}}{\eta}\Delta t\|p_0^{n+1}\|^2_{L^2(\Gamma_0)} + \left(\frac{\rho}{2}+\frac{R^2\tilde{c}\Delta t}{\eta}\right)\|\mathbf{u}^n\|^2_{L^2(\Omega)}.$$

The result follows from a discrete Gronwall lemma.

Proof of Result 2:

Assume that condition (10) is satisfied. Dealing with the product of integrals, using a trace inequality, Poincaré inequality and then Young inequality, we obtain:

$$\begin{aligned}\left|R\Delta t\left(\int_{\Gamma_1}\mathbf{u}^{n+1}\cdot\mathbf{n}\right)\left(\int_{\Gamma_1}\mathbf{u}^{n}\cdot\mathbf{n}\right)\right| &\leq \tilde{c}R\Delta t\|\nabla\mathbf{u}^{n+1}\|_{L^2(\Omega)}\|\nabla\mathbf{u}^n\|_{L^2(\Omega)},\\ &\leq \frac{\tilde{c}R\Delta t}{2}\left(\|\nabla\mathbf{u}^{n+1}\|^2_{L^2(\Omega)} + \|\nabla\mathbf{u}^n\|^2_{L^2(\Omega)}\right).\end{aligned} \tag{13}$$

Thanks to condition (10), we have $\frac{\eta\Delta t}{2} - \frac{\tilde{c}R\Delta t}{2} \geq \frac{\eta\Delta t}{4}$ and $\frac{\tilde{c}R\Delta t}{2} \leq \frac{\eta\Delta t}{4}$. With this and inserting Eq. (13) into Eq. (12), it holds:

$$\frac{\rho}{2}\|\mathbf{u}^{n+1}\|^2_{L^2(\Omega)} + \frac{\eta\Delta t}{4}\|\nabla\mathbf{u}^{n+1}\|^2_{L^2(\Omega)} \leq \frac{\rho}{2}\|\mathbf{u}^{n}\|^2_{L^2(\Omega)} + \frac{\eta\Delta t}{4}\|\nabla\mathbf{u}^{n}\|^2_{L^2(\Omega)} + \frac{\tilde{c}\Delta t}{2\eta}\|p_0^{n+1}\|^2_{L^2(\Gamma_0)}.$$

We now proceed by summation to get the desired result. Note that, in this case, we did not use Lemma 1 and thus the fact that $\mathrm{div}(\mathbf{u}^n)=0$ is not used. As a consequence, when considering the fully-discretized system in a forthcoming paragraph, a similar estimate will be derived, even if the divergence-free property is not satisfied.

Proof of Result 3:

We assume that Eq. (11) is satisfied. By Lemma 1 (since $\mathrm{div}(\mathbf{u}^n)=0$ for all n) and Young inequality, the product of integrals can be estimated as follows:

$$\begin{aligned}\left|R\Delta t\left(\int_{\Gamma_1}\mathbf{u}^{n+1}\cdot\mathbf{n}\right)\left(\int_{\Gamma_1}\mathbf{u}^{n}\cdot\mathbf{n}\right)\right| &\leq \tilde{c}R\Delta t\|\mathbf{u}^{n+1}\|_{L^2(\Omega)}\|\mathbf{u}^n\|_{L^2(\Omega)},\\ &\leq \frac{\tilde{c}R\Delta t}{2}\|\mathbf{u}^{n+1}\|^2_{L^2(\Omega)} + \frac{\tilde{c}R\Delta t}{2}\|\mathbf{u}^n\|^2_{L^2(\Omega)}.\end{aligned}$$

Then we get

$$\left(\frac{\rho}{2}-\frac{\tilde{c}R\Delta t}{2}\right)\|\mathbf{u}^{n+1}\|^2_{L^2(\Omega)} + \frac{\eta\Delta t}{2}\|\nabla\mathbf{u}^{n+1}\|^2_{L^2(\Omega)} \leq \frac{\tilde{c}\Delta t}{2\eta}\|p_0^{n+1}\|^2_{L^2(\Gamma_0)} + \left(\frac{\rho}{2}+\frac{\tilde{c}R\Delta t}{2}\right)\|\mathbf{u}^n\|^2_{L^2(\Omega)}.$$

Consequently, under the CFL condition $\frac{\rho}{2} - \frac{\tilde{c}R\Delta t}{2} > 0$ and unsing a discrete Gronwall lemma (see [24]), the result holds. □

Next let us underline the main differences between the semi-discretized system and the fully-discretized system when considering the numerical stability of the schemes. Let us first introduce some finite element spaces. Let $\mathcal{T}_h$ be a family of quasi-uniform triangulations $\mathcal{T}_h$ of Ω with mesh size h. For the space discretization, we introduce the spaces $\mathbf{V}_h$ and M_h as internal Lagrange finite element approximations of $\mathbf{V}$ and $L^2(\Omega)$, respectively. Note that if we consider the implicit coupling, it does not change the stability study and the solution of the fully-discretized problem satisfy estimates stated in Theorem 1, as the proof readily adapts. Thus we focus here on the finite element approximation of the semi-discrete explicit problem. The fully-discretized formulation, which we consider here, can be written as follows:

Scheme 3 (Fully-discretized Stokes problem with explicit coupling)**.** *Find* $(\mathbf{u}_h^{n+1}, p_h^{n+1})$ *in* $\mathbf{V}_h \times M_h$ *such that, for all* $(\mathbf{v}_h, q_h)$ *in* $\mathbf{V}_h \times M_h$*:*

$$\begin{aligned} &\frac{\rho}{\Delta t}\int_\Omega \mathbf{u}_h^{n+1}\cdot\mathbf{v}_h + \eta\int_\Omega \nabla\mathbf{u}_h^{n+1} : \nabla\mathbf{v}_h + \int_\Omega q_h \mathrm{div}(\mathbf{u}_h^{n+1}) + \int_\Omega p_h^{n+1}\mathrm{div}(\mathbf{v}_h) \\ &\qquad = \frac{\rho}{\Delta t}\int_\Omega \mathbf{u}_h^n\mathbf{v}_h - \int_{\Gamma_0} p_0^{n+1}\mathbf{v}_h\cdot\mathbf{n} - R\left(\int_{\Gamma_1}\mathbf{u}_h^n\cdot\mathbf{n}\right)\left(\int_{\Gamma_1}\mathbf{v}_h\cdot\mathbf{n}\right). \end{aligned} \tag{14}$$

The main difference between the fully-discretized problem (namely Scheme 3) and the semi-discretized problem (namely Scheme 1) comes from the fact that now $\mathbf{u}_h^{n+1}$ is not divergence free and consequently Lemma 1 cannot be used anymore. Indeed, when the fully-discretized system is considered we have only $\int_\Omega q_h \mathrm{div}(\mathbf{u}_h^{n+1}) = 0$, for all $q_h \in M_h$. However, for a well-chosen finite element approximation for the pressure, the flux of the fluid velocity at the outlet Γ_1 can be estimated thanks to the following result (analog to Lemma 1):

Lemma 2. *Let* $\mathbf{V}_h$ *and* M_h *be internal Lagrange finite element approximations of* $\mathbf{V}$ *and* $L^2(\Omega)$ *such that* M_h *contains an internal approximation space of* $H^1(\Omega)$*. Then, there exists a constant* $\tilde{c} > 0$ *such that, for all* $\mathbf{v}_h \in \mathbf{V}_h$ *satisfying*

$$\int_\Omega q_h \,\mathrm{div}(\mathbf{v}_h) = 0, \quad \forall q_h \in M_h,$$

then

$$\left|\int_{\Gamma_1}\mathbf{v}_h\cdot\mathbf{n}\right| \le \tilde{c}\|\mathbf{v}_h\|_{L^2(\Omega)}.$$

Proof. Thanks to Stokes formula, the flux term $\int_{\Gamma_1}\mathbf{v}_h\cdot\mathbf{n}$ can be defined by means of the standard duality as:

$$\int_{\Gamma_1}\mathbf{v}_h\cdot\mathbf{n} := \langle \mathbf{v}_h\cdot\mathbf{n}, g_h\rangle_{H^{-1/2}(\partial\Omega),H^{1/2}(\partial\Omega)} = \int_\Omega g_h\mathrm{div}(\mathbf{v}_h) + \int_\Omega \mathbf{v}_h\cdot\nabla g_h, \tag{15}$$

where g_h is any function belonging to X_h, defined as a continuous (thus internal) finite element approximation of $H^1(\Omega)$ included in M_h, and moreover g is such that $g_h = 1$ on Γ_1, $g_h = 0$ on Γ_0 and its gradient is bounded in L^2 independantly of h. Such a function exists since $\overline{\Gamma_0}\cap\overline{\Gamma_1} = \emptyset$. Note that $\mathbf{v}_h\cdot\mathbf{n}$ vanishes on the lateral boundary Γ_ℓ since $\mathbf{v}_h \in \mathbf{V}_h$. Moreover, we have $\int_\Omega q_h\mathrm{div}(\mathbf{v}_h) = 0$ for all q_h in M_h. Since we choose M_h containing X_h, (15) becomes:

$$\int_{\Gamma_1}\mathbf{v}_h\cdot\mathbf{n} = \int_\Omega \mathbf{v}_h\cdot\nabla g_h.$$

As the gradient of g_h is bounded in the L^2-norm independantly of h, the result holds. Note that the finite elements used for the pressure have to be at least $\mathbb{P}_1$ elements. □

If the finite element space M_h is such that Lemma 2 holds true, then all the estimates obtained for the semi-discretized system in Theorem 2 are still valid for the solution of the fully-discretized system (in particular *Results 1 and 3*). In the case where M_h does not contain a continuous finite element approximation of H^1 (e.g. using $\mathbb{P}_0$ finite elements for the pressure), then we can only obtain *Result 2* which is valid under a condition of smallness of the resistance R.

Remark 5. *It is possible to derive energy estimates without assuming that* R *is small enough. For instance, considering a regular family of triangulations* $\{\mathcal{T}_h\}$ *of* Ω*, it yields* [37]*:*

$$\forall \mathbf{v}_h \in \mathbf{V}_h, \quad \|\nabla\mathbf{v}_h\|_{L^2(\Omega)} \le \tilde{c}h^{-1}\|\mathbf{v}_h\|_{L^2(\Omega)}.$$

Using this inverse inequality together with a trace inequality, a discrete Gronwall lemma, and the following condition on the time-step:

$$\Delta t \le \frac{\rho h^2}{\tilde{c}R}, \tag{16}$$

we obtain an estimate of the L^2*-norm of the velocity approximation. However the upper bound has an exponential growth proportional to* $\exp(RT/h^2)$ *which is not relevant when* h *tends to zero.*

In the numerical test-cases performed at Section 5 (in particular Subsections 5.2 and 5.3, dedicated to Stokes flows), we will use continuous $\mathbb{P}_1$ finite elements for the pressure, hence guaranteeing that the solution of the fully-discretized problem with the explicit coupling not only satisfies *Result 2* of Theorem 2 but also satisfies the estimates derived in *Results 1* and *3* of Theorem 2. Consequently, in the following study of the RC and RCR models, we will only focus on the stability of the associated semi-discretized problems.

3.2. **RC model.** In the previous subsection, we studied a single R model. Here we are interested in extending the stability study to reduced models used in air flow modelling, see Section 2.2. Thus we consider the Stokes system, i.e. (1) without the convective term, with the RC reduced model defined by (2). Moreover we recall that, with no loss of generality, we consider the case $N_{\text{out}} = 1$. This system satifies a continous energy balance that can be obtained multiplying by $\mathbf{u}$ the first equation of (1) and by integrating over the domain Ω:

$$\frac{\mathrm{d}}{\mathrm{d}t}\left(\frac{\rho}{2}\int_\Omega |\mathbf{u}|^2\right) + \eta\int_\Omega |\nabla\mathbf{u}|^2 + \int_{\Gamma_0} p_0\mathbf{u}\cdot\mathbf{n} + R\left(\int_{\Gamma_1}\mathbf{u}\cdot\mathbf{n}\right)^2 + \frac{1}{C}\left(\int_0^t\int_{\Gamma_1}\mathbf{u}\cdot\mathbf{n}\right)\left(\int_{\Gamma_1}\mathbf{u}\cdot\mathbf{n}\right) = 0.$$

By Cauchy-Schwarz, Young, trace and Poincaré inequalities, we have

$$\left|\int_{\Gamma_0} p_0\mathbf{u}\cdot\mathbf{n}\right| \leq \frac{\eta}{2}\int_\Omega |\nabla\mathbf{u}|^2 + \frac{\tilde{c}}{2\eta}\int_{\Gamma_0}|p_0|^2. \tag{17}$$

Moreover, defining the volume of the removed part as $V(t) = \int_0^t\int_{\Gamma_1}\mathbf{u}\cdot\mathbf{n}$, the last term of the left hand side is equal to $\frac{1}{C}V(t)V'(t) = \frac{1}{2}[(V(t))^2]'$ and we easily get:

$$\frac{\rho}{2}\int_\Omega |\mathbf{u}(t,\cdot)|^2 + \frac{1}{2C}V(t) + \frac{\eta}{2}\int_0^t\int_\Omega |\nabla\mathbf{u}|^2 + R\int_0^t\left(\int_{\Gamma_1}\mathbf{u}\cdot\mathbf{n}\right)^2 \leq \frac{\rho}{2}\int_\Omega |\mathbf{u}(0,\cdot)|^2 + \frac{\tilde{c}}{2\eta}\int_0^t\int_{\Gamma_0}|p_0|^2.$$

Next we are going to derive the same kind of energy inequality in the discrete framework. Let us first consider the implicit scheme. If we discretize (2) in time with an implicit treatment and a basic quadrature method, we get the following boundary condition on Γ_1:

$$\eta\nabla\mathbf{u}^{n+1}\cdot\mathbf{n} - p^{n+1}\mathbf{n} = -F_{\Delta t}((Q^k)_{1\leq k\leq n+1})\mathbf{n}, \tag{18}$$

with

$$F_{\Delta t}((Q^k)_{1\leq k\leq n+1}) = RQ^{n+1} + \frac{\Delta t}{C}\sum_{k=1}^{n+1}Q^k. \tag{19}$$

As for the derivation of the continuous energy estimate, we introduce the discrete volume of the removed part at time t^n as

$$V^n := \sum_{k=1}^n \Delta t Q^k = \sum_{k=1}^n \Delta t\int_{\Gamma_1}\mathbf{u}^k\cdot\mathbf{n}, \quad n\geq 1, \tag{20}$$

and set $V^0 = 0$.

Theorem 3 (Implicit coupling for the RC model)**.** *The implicit scheme based on the variational formulation of Eq.* (5) *and Eqs.* (18), (19) *and* (20) *provides approximations* $\mathbf{u}^n, V^n$ *of the velocity field* $\mathbf{u}$ *and of the volume* V *such that:*

$$\frac{\rho}{2}\|\mathbf{u}^n\|^2_{L^2(\Omega)} + \frac{1}{2C}|V^n|^2 + \frac{\eta}{2}\sum_{k=1}^n\Delta t\|\nabla\mathbf{u}^k\|^2_{L^2(\Omega)} \leq \frac{\tilde{c}}{2\eta}\sum_{k=1}^n\Delta t\|p_0^k\|^2_{L^2(\Gamma_0)} + \frac{\rho}{2}\|\mathbf{u}^0\|^2_{L^2(\Omega)},$$

for all $n\in\{1,...,N\}$.

Proof. By multiplying the first equation of (5) by $\mathbf{u}^{n+1}$, integrating over Ω, performing an integration by parts and using the implicit coupling defined by Eq. (18), it holds, by using Eq. (9):

$$\begin{aligned}&\frac{\rho}{2}\|\mathbf{u}^{n+1}\|^2_{L^2(\Omega)} - \frac{\rho}{2}\|\mathbf{u}^n\|^2_{L^2(\Omega)} + \frac{\rho}{2}\|\mathbf{u}^{n+1}-\mathbf{u}^n\|^2_{L^2(\Omega)} + \frac{\eta\Delta t}{2}\|\nabla\mathbf{u}^{n+1}\|^2_{L^2(\Omega)}\\ &+ R\Delta t\left(\int_{\Gamma_1}\mathbf{u}^{n+1}\cdot\mathbf{n}\right)^2 + \frac{\Delta t^2}{C}\left(\int_{\Gamma_1}\mathbf{u}^{n+1}\cdot\mathbf{n}\right)\left(\sum_{k=1}^{n+1}\int_{\Gamma_1}\mathbf{u}^k\cdot\mathbf{n}\right) \leq \frac{\tilde{c}\Delta t}{2\eta}\|p_0^{n+1}\|^2_{L^2(\Gamma_0)}.\end{aligned} \tag{21}$$

Using the definition of the approximated flow Q^{n+1} and the definition of the approximated volume V^{n+1} (see Eq. (20)), we get:

$$\begin{aligned}\frac{\Delta t^2}{C}\left(\int_{\Gamma_1}\mathbf{u}^{n+1}\cdot\mathbf{n}\right)\left(\sum_{k=1}^{n+1}\int_{\Gamma_1}\mathbf{u}^{k}\cdot\mathbf{n}\right) &= \frac{\Delta t}{C}Q^{n+1}V^{n+1},\\ &= \frac{\Delta t}{C}\frac{V^{n+1}-V^n}{\Delta t}V^{n+1}.\end{aligned} \tag{22}$$

Injecting Eq. (22) into Eq. (21), it yields:

$$\frac{\rho}{2}\|\mathbf{u}^{n+1}\|^2_{L^2(\Omega)}+\frac{1}{C}|V^{n+1}|^2+\frac{\eta\Delta t}{2}\|\nabla\mathbf{u}^{n+1}\|^2_{L^2(\Omega)}\leq\frac{\tilde{c}\Delta t}{2\eta}\|p_0^{n+1}\|^2_{L^2(\Gamma_0)}+\frac{\rho}{2}\|\mathbf{u}^{n}\|^2_{L^2(\Omega)}+\frac{1}{C}|V^{n}|^2.$$

By summation, the proof is concluded. □

Next we focus on the explicit treatment of the RC model and we investigate whether the stability analysis for the RC model differs from the one obtained for the R model alone. If we discretize Eq. (2) in time with an explicit treatment, we get the following boundary condition on Γ_1:

$$\eta\nabla\mathbf{u}^{n+1}\cdot\mathbf{n}-p^{n+1}\mathbf{n}=-F_{\Delta t}((Q^k)_{0\leq k\leq n})\mathbf{n}, \tag{23}$$

with

$$F_{\Delta t}((Q^k)_{0\leq k\leq n})=\left(R+\frac{\Delta t}{C}\right)Q^n+\frac{\Delta t}{C}\sum_{k=0}^{n}Q^k. \tag{24}$$

Theorem 4 (Explicit coupling for the RC model)**.** *If the time-step satisfies:*

$$\Delta t<\frac{\tilde{c}\rho C}{RC+T}, \tag{25}$$

the explicit scheme based on the variational formulation of Eq. (5) *and Eqs.* (23) *and* (24) *provides an approximation* $\mathbf{u}^n$ *of the fluid velocity which satisfies the following discrete energy estimate:*

$$\frac{\rho}{2}\|\mathbf{u}^{n}\|^2_{L^2(\Omega)}+\frac{\eta}{2}\sum_{k=1}^{n}\Delta t\|\nabla\mathbf{u}^{k}\|^2_{L^2(\Omega)}\leq\tilde{c}\left(\frac{1}{2\eta}\sum_{k=1}^{n}\Delta t\|p_0^{k}\|^2_{L^2(\Gamma_0)}+\frac{\rho}{2}\|\mathbf{u}^{0}\|^2_{L^2(\Omega)}\right)\exp\left(\frac{2T(RC+T)}{\gamma\rho C}\right),$$

for all $n\in\{1,...,N\}$*, where* $\gamma=1-\dfrac{\Delta t}{\tilde{c}\rho C}(RC+T)>0$.

Proof. Once again multiplying the first equation of (5) by $\mathbf{u}^{n+1}$, integrating over Ω, performing an integration by parts and using the explicit couplig strategy defined by Eq. (23), it holds by Eq. (9):

$$\begin{aligned}&\frac{\rho}{2}\|\mathbf{u}^{n+1}\|^2_{L^2(\Omega)}-\frac{\rho}{2}\|\mathbf{u}^{n}\|^2_{L^2(\Omega)}+\frac{\rho}{2}\|\mathbf{u}^{n+1}-\mathbf{u}^{n}\|^2_{L^2(\Omega)}+\frac{\eta\Delta t}{2}\|\nabla\mathbf{u}^{n+1}\|^2_{L^2(\Omega)}\\ &+R\Delta t\left(\int_{\Gamma_1}\mathbf{u}^{n+1}\cdot\mathbf{n}\right)\left(\int_{\Gamma_1}\mathbf{u}^{n}\cdot\mathbf{n}\right)+\frac{\Delta t^2}{C}\left(\int_{\Gamma_1}\mathbf{u}^{n+1}\cdot\mathbf{n}\right)\left(\sum_{k=0}^{n}\int_{\Gamma_1}\mathbf{u}^{k}\cdot\mathbf{n}\right)\leq\frac{\tilde{c}\Delta t}{2\eta}\|p_0^{n+1}\|^2_{L^2(\Gamma_0)}.\end{aligned} \tag{26}$$

Using Young and Cauchy-Schwarz inequalities, Lemma 1 (since $\mathrm{div}(\mathbf{u}^n)=0$ for all n), the terms coming from the 0D model can be estimated as follows:

$$\begin{aligned}&\left|R\Delta t\left(\int_{\Gamma_1}\mathbf{u}^{n+1}\cdot\mathbf{n}\right)\left(\int_{\Gamma_1}\mathbf{u}^{n}\cdot\mathbf{n}\right)+\frac{\Delta t^2}{C}\left(\int_{\Gamma_1}\mathbf{u}^{n+1}\cdot\mathbf{n}\right)\left(\sum_{k=0}^{n}\int_{\Gamma_1}\mathbf{u}^{k}\cdot\mathbf{n}\right)\right|\\ &\leq\tilde{c}R\Delta t\|\mathbf{u}^{n+1}\|_{L^2(\Omega)}\|\mathbf{u}^{n}\|_{L^2(\Omega)}+\tilde{c}\sum_{k=0}^{n}\left(\frac{\Delta t^2}{C}\|\mathbf{u}^{n+1}\|_{L^2(\Omega)}\|\mathbf{u}^{k}\|_{L^2(\Omega)}\right)\\ &\leq\tilde{c}\frac{R\Delta t}{2}\left(\|\mathbf{u}^{n+1}\|^2_{L^2(\Omega)}+\|\mathbf{u}^{n}\|^2_{L^2(\Omega)}\right)+\tilde{c}\frac{T\Delta t}{2C}\|\mathbf{u}^{n+1}\|^2_{L^2(\Omega)}+\frac{\Delta t^2}{2C}\sum_{k=0}^{n}\|\mathbf{u}^{k}\|^2_{L^2(\Omega)}.\end{aligned} \tag{27}$$

with $\sum_{k=1}^{n}\Delta t\leq T$. Injecting Eq. (27) into Eq. (26), we obtain:

$$\begin{aligned}\frac{\rho}{2}\|\mathbf{u}^{n+1}\|^2_{L^2(\Omega)}+\frac{\eta\Delta t}{2}\|\nabla\mathbf{u}^{n+1}\|^2_{L^2(\Omega)}\leq\frac{\rho}{2}\|\mathbf{u}^{n}\|^2_{L^2(\Omega)}+\tilde{c}\Delta t\frac{RC+T}{2C}\|\mathbf{u}^{n+1}\|^2_{L^2(\Omega)}+\tilde{c}\frac{R\Delta t}{2}\|\mathbf{u}^{n}\|^2_{L^2(\Omega)}\\ +\frac{\tilde{c}\Delta t}{2\eta}\|p_0^{n+1}\|^2_{L^2(\Gamma_0)}+\tilde{c}\frac{\Delta t^2}{2C}\sum_{k=0}^{n}\|\mathbf{u}^{k}\|^2_{L^2(\Omega)}.\end{aligned}$$

We proceed by summation. This yields the following estimate:

$$\frac{\rho}{2}\|\mathbf{u}^{n+1}\|^2_{L^2(\Omega)} + \frac{\eta}{2}\sum_{k=1}^{n+1}\Delta t\|\nabla\mathbf{u}^k\|^2_{L^2(\Omega)} \leq \frac{\rho}{2}\|\mathbf{u}^0\|^2_{L^2(\Omega)} + \frac{\tilde{c}}{2\eta}\sum_{k=1}^{n+1}\Delta t\|p_0^k\|^2_{L^2(\Gamma_0)}$$
$$+\tilde{c}\frac{RC+T}{2C}\sum_{k=1}^{n+1}\Delta t\|\mathbf{u}^k\|^2_{L^2(\Omega)} + \tilde{c}\frac{R\Delta t}{2}\sum_{k=0}^{n}\|\mathbf{u}^k\|^2_{L^2(\Omega)} + \tilde{c}\sum_{k=0}^{n}\frac{\Delta t^2}{2C}\sum_{\ell=0}^{k}\|\mathbf{u}^\ell\|^2_{L^2(\Omega)}. \tag{28}$$

Since we have:

$$\sum_{k=0}^{n}\frac{\Delta t^2}{2C}\sum_{\ell=0}^{k}\|\mathbf{u}^\ell\|^2_{L^2(\Omega)} \leq (n+1)\frac{\Delta t^2}{2C}\sum_{\ell=0}^{n}\|\mathbf{u}^\ell\|^2_{L^2(\Omega)} \leq \frac{T}{2C}\sum_{k=0}^{n}\Delta t\|\mathbf{u}^k\|^2_{L^2(\Omega)}, \tag{29}$$

then, injecting Eq. (29) into Eq. (28), we obtain:

$$\frac{\rho}{2}\left(1-\tilde{c}\Delta t\frac{RC+T}{\rho C}\right)\|\mathbf{u}^{n+1}\|^2_{L^2(\Omega)} + \frac{\eta}{2}\sum_{k=1}^{n+1}\Delta t\|\nabla\mathbf{u}^k\|^2_{L^2(\Omega)}$$
$$\leq \frac{\rho}{2}\|\mathbf{u}^0\|^2_{L^2(\Omega)} + \frac{\tilde{c}}{2\eta}\sum_{k=1}^{n+1}\Delta t\|p_0^k\|^2_{L^2(\Gamma_0)} + \tilde{c}\frac{RC+T}{C}\sum_{k=0}^{n}\Delta t\|\mathbf{u}^k\|^2_{L^2(\Omega)}.$$

Assuming that the CFL condition (25) holds, the result holds by applying a discrete Gronwall lemma, see [24]. □

Consequently the explicit RC model is conditionally stable under a CFL condition involving the density of the fluid, the compliance of the reduced model, its characteristic relaxation time RC as well as the final time of simulation T. Note that a stability result without any constraint on the time step as in *Result 1* of Theorem 2, can be derived ; but the exponential growth is even worse, as $\exp(T^3)$.

Remark 6. *Note that when the compliance C goes to infinity (i. e. the elastance goes to zero) in Eq.* (25)*, one recovers the CFL condition* (11) *obtained in* Result 3 *for the R model alone. Consequently both results are consistant.*

Remark 7. *The CFL condition* (25) *is unusual because it depends on the final time T resulting in a sharp limitation to long-time simulations. Nevertheless we did not experience such a limitation in practical simulations.*

3.3. **RCR model.** We now study the RCR model which is adapted for blood flow modelling. Considering the Stokes system, i.e. (1) without the convective term and with $N_{\text{out}} = 1$, with the reduced model given by (3), the energy balance can be obtained by multiplying by $\mathbf{u}$ the first equation of (1), by P_{d} the first equation of (3) and by Q the second equation of (3) and by recalling that $p_1(t) = F(Q(s), 0 \leq s \leq t) = P_{\text{d}}(t)$:

$$\frac{\mathrm{d}}{\mathrm{d}t}\left(\frac{\rho}{2}\int_\Omega|\mathbf{u}|^2 + CP_{\text{d}}^2\right) + \eta\int_\Omega|\nabla\mathbf{u}|^2 + \int_{\Gamma_0}p_0\mathbf{u}\cdot\mathbf{n} + R_{\text{p}}\left(\int_{\Gamma_1}\mathbf{u}\cdot\mathbf{n}\right)^2 + \frac{P_{\text{d}}^2}{R_{\text{d}}} = 0.$$

Then we easily get, by Eq. (17) and the Gronwall Lemma:

$$\frac{\rho}{2}\int_\Omega|\mathbf{u}(t,\cdot)|^2 + CP_{\text{d}}(t)^2 + \frac{\eta}{2}\int_0^t\int_\Omega|\nabla\mathbf{u}|^2 + R\int_0^t\left(\int_{\Gamma_1}\mathbf{u}\cdot\mathbf{n}\right)^2 + \int_0^t\frac{P_{\text{d}}^2}{R_{\text{d}}}$$
$$\leq \frac{\rho}{2}\int_\Omega|\mathbf{u}(0,\cdot)|^2 + CP_{\text{d}}^2(0) + \frac{\tilde{c}}{2\eta}\int_0^t\int_{\Gamma_0}|p_0|^2.$$

The energy balance highlights two types of dissipated powers: within the proximal part of the removed subtree, $R(\int_{\Gamma_1}\mathbf{u}\cdot\mathbf{n})^2$, and within the distal part of the removed subtree, $P_{\text{d}}^2/R_{\text{d}}$.

In this subsection, we investigate the numerical stability of the Stokes system for the RCR reduced model and two different coupling strategies. Let us first consider an implicit coupling. We discretize the system (3) for only one outlet, as follows

$$\begin{cases} P_{\text{p}}^{n+1} = R_{\text{p}}Q_{n+1} + P_{\text{d}}^{n+1}, \\ C\dfrac{P_{\text{d}}^{n+1}-P_{\text{d}}^n}{\Delta t} + \dfrac{P_{\text{d}}^{n+1}}{R_{\text{d}}} = Q^{n+1}. \end{cases} \tag{30}$$

Theorem 5 (Implicit coupling for the RCR model)**.** *The implicit scheme* (5) *(i.e with $m = n+1$) with $F_{\Delta t}((Q^k)_{0\leq k\leq n+1}) = P_{\text{p}}^{n+1}$, where P_{p}^{n+1} is the solution of* (30)*, provides an approximation $\mathbf{u}^n$ of the fluid velocity such that:*

$$\frac{\rho}{2}\|\mathbf{u}^n\|^2_{L^2(\Omega)} + \frac{C}{2}|P_{\text{d}}^n|^2 + R_{\text{p}}\sum_{k=1}^{n}\Delta t\left(\int_{\Gamma_1}\mathbf{u}^k\cdot\mathbf{n}\right)^2 + \sum_{k=1}^{n}\Delta t\frac{(P_{\text{d}}^k)^2}{R_{\text{d}}} + \frac{\eta}{2}\sum_{k=1}^{n}\Delta t\|\nabla\mathbf{u}^k\|^2_{L^2(\Omega)}$$
$$\leq \frac{\tilde{c}}{2\eta}\sum_{k=1}^{n}\Delta t\|p_0^k\|^2_{L^2(\Gamma_0)} + \frac{\rho}{2}\|\mathbf{u}^0\|^2_{L^2(\Omega)} + \frac{C}{2}(P_{\text{d}}^0)^2.$$

for all $n \in \{1, ..., N\}$.

Proof. Multiplying the first equation of (30) by Q^{n+1} and the second one by $P_{\rm d}^{n+1}$, we get:

$$P_{\rm p}^{n+1}Q^{n+1} = R_{\rm p}(Q^{n+1})^2 + \frac{C}{2\Delta t}\left((P_{\rm d}^{n+1})^2 - (P_{\rm d}^{n})^2 + (P_{\rm d}^{n+1} - P_{\rm d}^{n})^2\right) + \frac{(P_{\rm d}^{n+1})^2}{R_{\rm d}}. \tag{31}$$

Once again multiplying the first equation of (5) by $\mathbf{u}^{n+1}$, integrating over the domain Ω, integrating by parts, and using (31) and (9), leads to:

$$\begin{aligned}
&\frac{\rho}{2}\|\mathbf{u}^{n+1}\|^2_{L^2(\Omega)} - \frac{\rho}{2}\|\mathbf{u}^{n}\|^2_{L^2(\Omega)} + \frac{\rho}{2}\|\mathbf{u}^{n+1} - \mathbf{u}^{n}\|^2_{L^2(\Omega)} \\
&+ \Delta t\frac{\eta}{2}\|\nabla\mathbf{u}^{n+1}\|^2_{L^2(\Omega)} + R_{\rm p}\Delta t\left(\int_{\Gamma_1}\mathbf{u}^{n+1}\cdot\mathbf{n}\right)^2 + \Delta t\frac{(P_{\rm d}^{n+1})^2}{R_{\rm d}} \\
&+ \frac{C}{2}(P_{\rm d}^{n+1})^2 - \frac{C}{2}(P_{\rm d}^{n})^2 + \frac{C}{2}(P_{\rm d}^{n+1} - P_{\rm d}^{n})^2 \leq \frac{\tilde{c}}{2\eta}\Delta t\|p_0^{n+1}\|^2_{L^2(\Gamma_0)}.
\end{aligned}$$

The result is obtained by summation. □

Consequently, and not surprisingly, the considered implicit scheme is unconditionally stable. Let us now study an explicit coupling. We discretize the system (3) for only one outlet ($N_{\rm out} = 1$) as follows

$$\begin{cases} P_{\rm p}^{n+1} = R_{\rm p}Q^{n} + P_{\rm d}^{n+1}, \\ C\dfrac{P_{\rm d}^{n+1} - P_{\rm d}^{n}}{\Delta t} + \dfrac{P_{\rm d}^{n+1}}{R_{\rm d}} = Q^{n}. \end{cases} \tag{32}$$

This discretization is explicit since the proximal pressure $P_{\rm d}^{n+1}$ can be computed from the fluid flux Q^n at the previous time step. Consequently $P_{\rm d}^{n+1} = F_{\Delta t}((Q^k)_{0\leq k\leq n})$.

Theorem 6 (Explicit coupling for the RCR model)**.** *Under the assumption*

$$\Delta t \leq \tilde{c}\frac{\rho}{R_{\rm d}}, \tag{33}$$

the explicit scheme (5) *(i. e. with* $m = n$*) with* $F_{\Delta t}((Q^k)_{0\leq k\leq n}) = P_{\rm p}^{n+1}$*,* $P_{\rm p}^{n+1}$ *being solution of* (32)*, provides an approximation* $\mathbf{u}^n$ *of the fluid velocity such that:*

(i) *the following energy estimate is satisfied*

$$\begin{aligned}
&\frac{\rho}{2}\|\mathbf{u}^{n}\|^2_{L^2(\Omega)} + \frac{C}{2}|P_{\rm d}^{n}|^2 + \frac{\eta}{4}\sum_{k=1}^{n}\Delta t\|\nabla\mathbf{u}^{k}\|^2_{L^2(\Omega)} + \frac{\Delta t}{2}\frac{(P_{\rm d}^{n+1})^2}{R_{\rm d}} \\
&\quad\leq \left(\frac{\tilde{c}}{\eta}\sum_{k=1}^{n}\Delta t\|p_0^{k}\|^2_{L^2(\Gamma_0)} + \frac{\rho}{2}\|\mathbf{u}^{0}\|^2_{L^2(\Omega)} + \frac{C}{2}(P_{\rm d}^{0})^2\right)\exp\left(\frac{\tilde{c}R_{\rm p}^2T}{\eta}\right),\ 1\leq n\leq N.
\end{aligned}$$

(ii) *if moreover* $\eta \geq \widetilde{c}R_{\rm p}$*, the following energy estimate is satisfied*

$$\begin{aligned}
&\frac{\rho}{2}\|\mathbf{u}^{n}\|^2_{L^2(\Omega)} + \frac{C}{2}|P_{\rm d}^{n}|^2 + \frac{\eta\Delta t}{4}\|\nabla\mathbf{u}^{n}\|^2_{L^2(\Omega)} + \frac{\Delta t}{2}\frac{(P_{\rm d}^{n+1})^2}{R_{\rm d}} \\
&\quad\leq \frac{\tilde{c}}{\eta}\sum_{k=1}^{n}\Delta t\|p_0^{k}\|^2_{L^2(\Gamma_0)} + \frac{\rho}{2}\|\mathbf{u}^{0}\|^2_{L^2(\Omega)} + \frac{C}{2}(P_{\rm d}^{0})^2 + \frac{\eta\Delta t}{4}\|\nabla\mathbf{u}^{0}\|^2_{L^2(\Omega)},\quad 1\leq n\leq N.
\end{aligned}$$

(iii) *if the time-step satisfies the following additional condition:*

$$\Delta t < \widetilde{c}\frac{\rho}{R_{\rm p}},$$

then, the following energy estimate is satisfied for $1 \leq n \leq N$

$$\begin{aligned}
&\frac{\rho}{2}\|\mathbf{u}^{n}\|^2_{L^2(\Omega)} + \frac{C}{2}|P_{\rm d}^{n}|^2 + \frac{\eta}{2}\sum_{k=1}^{n}\Delta t\|\nabla\mathbf{u}^{k}\|^2_{L^2(\Omega)} + \frac{\Delta t}{2}\frac{(P_{\rm d}^{n+1})^2}{R_{\rm d}} \\
&\quad\leq \left(\frac{\tilde{c}}{\eta}\sum_{k=1}^{n}\Delta t\|p_0^{k}\|^2_{L^2(\Gamma_0)} + \frac{\rho}{2}\|\mathbf{u}^{0}\|^2_{L^2(\Omega)} + \frac{C}{2}(P_{\rm d}^{0})^2\right)\exp\left(\frac{\tilde{c}R_{\rm p}T}{\gamma}\right),
\end{aligned}$$

where $\gamma = 1 - \frac{\tilde{c}R_{\rm p}\Delta t}{\rho} > 0$.

Proof. Multiplying the first equation of (32) by Q^{n+1}, the second one by $P_{\rm d}^{n+1}$ and summing these two contributions, we get:

$$P_{\rm p}^{n+1}Q^{n+1} = R_{\rm p}Q^nQ^{n+1} + P_{\rm d}^{n+1}(Q^{n+1}-Q^n) + \frac{C}{2\Delta t}\left((P_{\rm d}^{n+1})^2 - (P_{\rm d}^n)^2 + (P_{\rm d}^{n+1}-P_{\rm d}^n)^2\right) + \frac{(P_{\rm d}^{n+1})^2}{R_{\rm d}}. \tag{34}$$

Using (34) and performing the very same steps as in the implicit case, we obtain:

$$\frac{\rho}{2}\|\mathbf{u}^{n+1}\|^2_{L^2(\Omega)} - \frac{\rho}{2}\|\mathbf{u}^n\|^2_{L^2(\Omega)} + \frac{\rho}{2}\|\mathbf{u}^{n+1}-\mathbf{u}^n\|^2_{L^2(\Omega)} + \Delta t P_{\rm d}^{n+1}\left(\int_{\Gamma_1}(\mathbf{u}^{n+1}-\mathbf{u}^n)\cdot\mathbf{n}\right)$$
$$+ \Delta t\frac{\eta}{2}\|\nabla\mathbf{u}^{n+1}\|^2_{L^2(\Omega)} + R_{\rm p}\Delta t\left(\int_{\Gamma_1}\mathbf{u}^{n+1}\cdot\mathbf{n}\right)\left(\int_{\Gamma_1}\mathbf{u}^n\cdot\mathbf{n}\right) + \Delta t\frac{(P_{\rm d}^{n+1})^2}{R_{\rm d}}$$
$$+ \frac{C}{2}(P_{\rm d}^{n+1})^2 - \frac{C}{2}(P_{\rm d}^n)^2 + \frac{C}{2}(P_{\rm d}^{n+1}-P_{\rm d}^n)^2 \le \frac{\tilde{c}}{2\eta}\Delta t\|p_0^{n+1}\|^2_{L^2(\Gamma_0)}.$$

We remark that we have two terms to deal with. The first one is $R_{\rm p}\Delta t(\int_{\Gamma_1}\mathbf{u}^{n+1}\cdot\mathbf{n})(\int_{\Gamma_1}\mathbf{u}^n\cdot\mathbf{n})$ which already appears in the study of the explicit scheme for R model. The second one is new and writes $\Delta t P_{\rm d}^{n+1}\left(\int_{\Gamma_1}(\mathbf{u}^{n+1}-\mathbf{u}^n)\cdot\mathbf{n}\right)$. Thanks to Lemma 1 and Young inequality, we easily estimate it:

$$\left|\Delta t P_{\rm d}^{n+1}\left(\int_{\Gamma_1}(\mathbf{u}^{n+1}-\mathbf{u}^n)\cdot\mathbf{n}\right)\right| \le \tilde{c}\Delta t|P_{\rm d}^{n+1}|\ \|\mathbf{u}^{n+1}-\mathbf{u}^n\|_{L^2(\Omega)},$$
$$\le \frac{\Delta t}{2}\frac{|P_{\rm d}^{n+1}|^2}{R_{\rm d}} + \tilde{c}\Delta t R_{\rm d}\|\mathbf{u}^{n+1}-\mathbf{u}^n\|^2_{L^2(\Omega)}.$$

Consequently, under condition (33), these terms are absorbed by the left-hand side. Next proceeding as in the proof of Theorem 2 to deal with the term $R_{\rm p}\Delta t(\int_{\Gamma_1}\mathbf{u}^{n+1}\cdot\mathbf{n})(\int_{\Gamma_1}\mathbf{u}^n\cdot\mathbf{n})$, the three results hold true. □

Remark 8. *Few remarks are in order. The first one is that, once the additional condition* (33) *on the time step that involves the quotient* $\frac{\rho}{R_{\rm d}}$ *is assumed to hold true, the results are the same as for the R model in Theorem 2. The second one is that none of the necessary conditions that have been presented involves the compliance C, unlike for the RC model (see condition* (25)*). Moreover the exponential growth behaves like* $\exp(T)$ *and not* $\exp(T^2)$ *or even* $\exp(T^3)$ *as in the RC model case.*

Remark 9. *The authors of* [6] *studied the stability of these RCR non-local boundary conditions with a projection fractional step scheme* [8, 9, 39, 40, 22] *for the discretization of the Stokes system. When considering an explicit coupling, an uncontrolled artificial power appears which does not guarantee the energy stability of the approximation provided by the explicit scheme, except in the case of a single outlet. Using an implicit coupling allows to bound the energy, and then guarantees the numerical stability of the approximation.*

4. Navier-Stokes system and reduced models

In Section 3, the Stokes system has been considered. In this section, we underline the difficulties met when one is interested in analyzing the numerical stability of these systems considering Navier-Stokes equations and thus adding nonlinearities to the problem, because of the inertial effects. Let us first review the difficulties coming from the convection terms in the continuous framework. To fix the idea we consider the Navier-Stokes system (1) with a single outlet (N_{out}=1) coupled with a R model so that $F(Q(s), 0\le s\le t) = RQ(t)$ according to the notations that were previously introduced. By multiplying the first equation of (1) by the fluid velocity $\mathbf{u}$, integrating over the domain Ω and integrating by parts, we obtain, at least formally, the following energy equality:

$$\frac{\rho}{2}\frac{\mathrm{d}}{\mathrm{d}t}\int_\Omega|\mathbf{u}|^2 + \rho\int_{\Gamma_0\cup\Gamma_1}\frac{|\mathbf{u}|^2}{2}\mathbf{u}\cdot\mathbf{n} + \eta\int_\Omega|\nabla\mathbf{u}|^2 + R\left(\int_{\Gamma_1}\mathbf{u}\cdot\mathbf{n}\right)^2 = \int_{\Gamma_0}p_0\mathbf{u}\cdot\mathbf{n}$$

Here we have used the prescribed Neumann boundary condition on Γ_0, the coupling with the R model, as well as the divergence free property. We see a boundary term $\rho\int_{\Gamma_0\cup\Gamma_1}\frac{|\mathbf{u}|^2}{2}\mathbf{u}\cdot\mathbf{n}$ that represents the flux of kinetic energy at the artificial boundaries, whose sign is not known *a priori*. Consequently, unlike in the Stokes system, one can not derive an energy estimate so easily. To obtain a satisfactory energy estimate and existence theorems, one has to be able to control this kinetic energy flux at the interface where Neumann boundary conditions are prescribed. Note that in 3D we can prove the following bound (see [25])

$$\left|\rho\int_{\Gamma_0\cup\Gamma_1}\frac{|\mathbf{u}|^2}{2}\mathbf{u}\cdot\mathbf{n}\right| \le C\|\mathbf{u}\|^{5/2}_{L^2(\Omega)}\|\nabla\mathbf{u}\|^{1/2}_{L^2(\Omega)},$$

which does not allow to obtain an energy estimate. Nevertheless existence of a unique strong solution can be proven. In particular, in [2], the existence of a unique strong solution (locally in time or for small data) is

derived, based on the same ideas developped in [25] and on regularity results of the solution of the stationnary Stokes system with mixed Dirichlet-Neumann boundary conditions in polyhedral domains [32]. The proof of existence of a strong solution is based on a Galerkin method with a special and well-chosen basis. We will use the same idea to derive an existence result together with stability estimates for the semi-discretized system. The Galerkin basis is linked to a modified Stokes operator A_R which will be defined thereafter. Note that we currently focus on the Navier-Stokes system coupled to the R model. We denote by $a_R(\cdot,\cdot)$ the inner product on $\mathbf{V}_{\rm div} \times \mathbf{V}_{\rm div}$ defined by

$$a_R(\mathbf{u},\mathbf{v}) = \eta\,(\nabla\mathbf{u},\nabla\mathbf{v})_\Omega + R\left(\int_{\Gamma_1}\mathbf{u}\cdot\mathbf{n}\right)\left(\int_{\Gamma_1}\mathbf{v}\cdot\mathbf{n}\right)$$

and $|||\cdot|||$ its associated norm ($R \geq 0$). Note that this norm and the semi-norm $\mathbf{H}^1$ are equivalent in $\mathbf{V}$ and then in $\mathbf{V}_{\rm div}$. We introduce the modified Stokes operator $A_R:\ \mathcal{D}(A_R) \subset \mathbf{H} \longrightarrow \mathbf{H}$ as follows:

- $\mathcal{D}(A_R) = \{\mathbf{u} \in \mathbf{V}_{\rm div},\ |a_R(\mathbf{u},\mathbf{v})| \leq \tilde{c}\|\mathbf{u}\|_{L^2(\Omega)},\ \forall \mathbf{v} \in \mathbf{V}_{\rm div}\}$,
- $\forall \mathbf{u} \in \mathcal{D}(A_R),\ (A_R\mathbf{u},\mathbf{v})_\Omega = a_R(\mathbf{u},\mathbf{v}),\ \forall \mathbf{v} \in \mathbf{V}_{\rm div}$.

A key result used to prove the existence of a strong solution is the following lemma (see [2]):

Lemma 3. *If the boundaries Γ_0 and Γ_1 meet the lateral boundaries Γ_ℓ at angle $\pi/2$, then there exists $c_1 > 0$, such that, for $\mathbf{u} \in \mathcal{D}(A_R)$*

$$\|\mathbf{u}\|_{L^\infty(\Omega)} \leq \frac{c_1}{\eta}\|A_R\mathbf{u}\|_{L^2(\Omega)}.$$

Note that Lemma 3 relies on the fact that there exists $\varepsilon > 0$ such that $\mathcal{D}(A_R) \subset \mathbf{H}^{3/2+\varepsilon}(\Omega)$. For this result to hold true, the boundaries Γ_0 and Γ_1 have to meet the lateral boundaries Γ_ℓ at angle $\pi/2$. Moreover the dependancy of the constant with respect to the physical parameters can be obtain by considering the operator $A = \eta^{-1}A_R$ that depends only on the purely geometric coeficient R/η and by noting that any solution of $A_R\mathbf{u} = \mathbf{f}$ is a solution of $A\mathbf{u} = \frac{\mathbf{f}}{\eta}$.

By taking $\mathbf{v} = A_R\mathbf{u}$ as a test-function for the continuous problem and by using Lemma 3, one can prove, at least formally, that $\mathbf{u} \in L^\infty(0,T;\mathbf{V}) \cap L^2(0,T;\mathcal{D}(A_R))$. A rigorous justification of this property and the proof of existence of a strong solution rely on the consideration of the eigenfunctions of the operator A_R as a Galerkin basis.

In what follows, we study the existence (and stability estimates) of a unique strong solution of the semi-discretized system. For the sake of simplicity, we assume that the applied pressure p_0 only depends on time. Nevertheless, all the results presented below are still valid assuming that $p_0 \in H^{1/2}(\Gamma_0)$ and by remplacing the condition of smallness over $|p_0|$ by a condition of smallness over $\|p_0\|_{H^{1/2}(\Gamma_0)}$. Dealing with the implicit treatment for the R reduced model and with the full-implicit scheme for the convective term, the problem can be written as:

$$\left\{\begin{array}{rcll}
\rho\dfrac{\mathbf{u}^{n+1}-\mathbf{u}^n}{\Delta t} + \rho(\mathbf{u}^{n+1}\cdot\nabla)\mathbf{u}^{n+1} - \eta\Delta\mathbf{u}^{n+1} + \nabla p^{n+1} &=& 0 & \text{in } \Omega,\\
\operatorname{div}(\mathbf{u}^{n+1}) &=& 0 & \text{in } \Omega,\\
\mathbf{u}^{n+1} &=& 0 & \text{on } \Gamma_\ell,\\
\eta\nabla\mathbf{u}^{n+1}\cdot\mathbf{n} - p^{n+1}\mathbf{n} &=& -p_0^{n+1}\mathbf{n} & \text{on } \Gamma_0,\\
\eta\nabla\mathbf{u}^{n+1}\cdot\mathbf{n} - p^{n+1}\mathbf{n} &=& -(R\int_{\Gamma_1}\mathbf{u}^{n+1}\cdot\mathbf{n})\mathbf{n} & \text{on } \Gamma_1,\\
\mathbf{u}^0 &=& \mathbf{u}_0 & \text{in } \Omega.
\end{array}\right. \tag{35}$$

The corresponding variational formulation is:

Scheme 4 (Semi-discretized R model for the Navier-Stokes problem with implicit coupling)**.** *Let $\mathbf{u}^0 = \mathbf{u}_0 \in \mathbf{V}_{\rm div}$ be the initial data. Find $\mathbf{u}^{n+1}$ in $\mathbf{V}_{\rm div}$ such that, for all $\mathbf{v}$ in $\mathbf{V}_{\rm div}$:*

$$\begin{aligned}\frac{\rho}{\Delta t}\int_\Omega \mathbf{u}^{n+1}\cdot\mathbf{v} + \rho\int_\Omega(\mathbf{u}^{n+1}\cdot\nabla)\mathbf{u}^{n+1}\cdot\mathbf{v} + \eta\int_\Omega\nabla\mathbf{u}^{n+1}:\nabla\mathbf{v} + R\left(\int_{\Gamma_1}\mathbf{u}^{n+1}\cdot\mathbf{n}\right)\left(\int_{\Gamma_1}\mathbf{v}\cdot\mathbf{n}\right)\\ = \frac{\rho}{\Delta t}\int_\Omega\mathbf{u}^n\cdot\mathbf{v} - p_0^{n+1}\int_{\Gamma_0}\mathbf{v}\cdot\mathbf{n}.\end{aligned} \tag{36}$$

This semi-discrete problem suffers from the same drawback as previously: one can not derive energy bound by taking $\mathbf{v} = \mathbf{u}^{n+1}$ as a test function. However, we have the following existence theorem:

Theorem 7 (Existence)**.** *Assuming that the initial and boundary data are sufficiently small, namely*

$$\frac{\rho}{2}|||\mathbf{u}^0|||^2 + \frac{\Delta t}{2}\sum_{k=1}^N |p_0^k|^2 \leq \frac{\alpha^2\eta^3}{8c_1\rho}, \tag{37}$$

and defining the ball B_α by

$$B_\alpha = \left\{\mathbf{v} \in \mathrm{V}_{\rm div}, \|\nabla\mathbf{v}\|_{L^2(\Omega)} \leq \frac{\alpha\eta}{2c_1\rho},\right\},\ 0 < \alpha < 1, \tag{38}$$

then Scheme 4 has a solution in B_α and defines a sequence of solutions $\mathbf{u}^n$ that satisfies

$$\frac{\rho}{2}|||\mathbf{u}^n|||^2 + (1-\alpha)\frac{\Delta t}{2}\sum_{k=1}^{n}\|A_R\mathbf{u}^k\|^2_{L^2(\Omega)} \leq \frac{\rho}{2}|||\mathbf{u}^0|||^2 + \frac{\Delta t}{2}\sum_{k=1}^{n}|p_0^k|^2, \tag{39}$$

for all $n \in \{1, ..., N\}$.

Remark 10. *The smallness condition* (37) *on the applied data to obtain the existence of a solution is really restrictive and its order of magnitude strongly depends on the considered application.*

Proof. The proof of existence of a solution of Eqs. (35) relies on a fixed-point argument: a Galerkin method for a well-chosen basis and the derivation of estimates satisfied by any solution, provided the data are small enough. Let n be fixed. Let us assume that $\mathbf{u}^n$ is given and satisfies, together with p_0^{n+1},

$$\frac{\Delta t}{2}|p_0^{n+1}|^2 + \frac{\rho}{2}|||\mathbf{u}^n|||^2 \leq \frac{\alpha^2\eta^3}{8c_1\rho}. \tag{40}$$

Let us first define the Galerkin basis. The operator A_R is self-adjoint and its inverse is compact on $\mathbf{H}$. Therefore, it admits a sequence of eigenfunctions $\{\mathbf{a}_k\}_{k\geq 0}$, which is complete and orthogonal both in $\mathbf{V}_{\rm div}$ and $\mathbf{H}$. The family $\{\mathbf{a}_k\}_{0\leq k\leq m}$ is chosen as a special Galerkin basis. We denote $\mathbf{V}_m = \text{span}\{\mathbf{a}_k\}_{0\leq k\leq m}$, which is used to build our sequence of approximate solutions $(\mathbf{u}_m^{n+1})_{m\geq 0}$ of (35). The approximate solution $\mathbf{u}_m^{n+1} = \sum_{i=1}^m c_{n+1,m,i}\mathbf{a}_i \in \mathbf{V}_m$ solves the following variational problem:

Scheme 5. *Let $\mathbf{u}^n \in \mathbf{V}_{\rm div}$. Find $\mathbf{u}_m^{n+1}$ in $\mathbf{V}_m$ such that, for all $\mathbf{v}$ in $\mathbf{V}_m$:*

$$\begin{aligned}\frac{\rho}{\Delta t}\int_\Omega \mathbf{u}_m^{n+1}\cdot\mathbf{v} + \rho\int_\Omega(\mathbf{u}_m^{n+1}\cdot\nabla)\mathbf{u}_m^{n+1}\cdot\mathbf{v} + \eta\int_\Omega\nabla\mathbf{u}_m^{n+1}:\nabla\mathbf{v}\\ +R\left(\int_{\Gamma_1}\mathbf{u}_m^{n+1}\cdot\mathbf{n}\right)\left(\int_{\Gamma_1}\mathbf{v}\cdot\mathbf{n}\right) = \frac{\rho}{\Delta t}\int_\Omega\mathbf{u}^n\mathbf{v} - p_0^{n+1}\int_{\Gamma_0}\mathbf{v}\cdot\mathbf{n}.\end{aligned}$$

We prove that Scheme 5 has a solution thanks to a Brouwer's fixed point Theorem applied to the mapping $T : \mathbf{w} \in B_\alpha \cap \mathbf{V}_m \longmapsto \mathbf{z}_m^{n+1} \in \mathbf{V}_m$, where $\mathbf{z}_m^{n+1}$ is defined by the following linear problem:

Scheme 6. *Let $\mathbf{u}^n \in \mathbf{V}_{\rm div}$. Find $\mathbf{z}_m^{n+1}$ in $\mathbf{V}_m$ such that:*

$$\begin{aligned}\rho\left(\mathbf{z}_m^{n+1},\mathbf{v}\right)_\Omega + \Delta t\ a_R(\mathbf{z}_m^{n+1},\mathbf{v}) + \rho\Delta t\left((\mathbf{z}_m^{n+1}\cdot\nabla)\mathbf{w},\mathbf{v}\right)_\Omega\\ = \rho\left(\mathbf{u}^n,\mathbf{v}\right)_\Omega - \Delta t p_0^{n+1}\int_{\Gamma_0}\mathbf{v}\cdot\mathbf{n},\ \forall\mathbf{v}\in\mathbf{V}_m.\end{aligned}$$

One can easily prove that Scheme 6 has a unique solution $\mathbf{z}_m^{n+1} \in \mathbf{V}_m$. The mapping T is clearly continuous on $\mathbf{V}_m$. To apply Brouwer's fixed point Theorem we are going to verify that $T(B_\alpha\cap\mathbf{V}_m) \subset B_\alpha\cap\mathbf{V}_m$ where B_α is defined by (38). Choosing $\mathbf{v} = A_R\mathbf{z}_m^{n+1}$ as a test function, which is admissible since $A_R\mathbf{z}_m^{n+1} \in \mathbf{V}_m$ thanks to the choice of the Galerkin basis, we get:

$$\begin{aligned}&\rho\ a_R(\mathbf{z}_m^{n+1},\mathbf{z}_m^{n+1}) + \Delta t\ \|A_R\mathbf{z}_m^{n+1}\|^2_{L^2(\Omega)}\\ &+\rho\Delta t\left((\mathbf{z}_m^{n+1}\cdot\nabla)\mathbf{w}, A_R\mathbf{z}_m^{n+1}\right)_\Omega = \rho\ a_R(\mathbf{u}_m^n,\mathbf{z}_m^{n+1}) - \Delta t p_0^{n+1}\int_{\Gamma_0}A_R\mathbf{z}_m^{n+1}\cdot\mathbf{n}.\end{aligned}$$

Since $A_R\mathbf{z}_m^{n+1}$ is divergence free, we can apply Lemma 1 to get:

$$\left|\Delta t p_0^{n+1}\int_{\Gamma_0}A_R\mathbf{z}_m^{n+1}\cdot\mathbf{n}\right| \leq \frac{\Delta t}{2}\left(|p_0|^2 + \|A_R\mathbf{z}_m^{n+1}\|^2_{L^2(\Omega)}\right). \tag{41}$$

The convective term can be estimated as follows:

$$\left|\rho\Delta t\left((\mathbf{z}_m^{n+1}\cdot\nabla)\mathbf{w}, A_R\mathbf{z}_m^{n+1}\right)_\Omega\right| \leq \rho\Delta t\|\mathbf{z}_m^{n+1}\|_{L^\infty(\Omega)}\|\nabla\mathbf{w}\|_{L^2(\Omega)}\|A_R\mathbf{z}_m^{n+1}\|_{L^2(\Omega)}. \tag{42}$$

Then using Lemma 3, one gets $\|\mathbf{z}_m^{n+1}\|_{L^\infty(\Omega)} \leq \frac{c_1}{\eta}\|A_R\mathbf{z}_m^{n+1}\|_{L^2(\Omega)}$. It yields:

$$\frac{\rho}{2}|||\mathbf{z}_m^{n+1}|||^2 + \Delta t\left(\frac{1}{2} - \frac{c_1\rho}{\eta}\|\nabla\mathbf{w}\|_{L^2(\Omega)}\right)\|A_R\mathbf{z}_m^{n+1}\|^2_{L^2(\Omega)} \leq \frac{\Delta t}{2}|p_0^{n+1}|^2 + \frac{\rho}{2}|||\mathbf{u}^n|||^2.$$

As $\mathbf{w} \in B_\alpha$, we obtain thanks to (37) the following estimate:

$$\frac{\rho}{2}|||\mathbf{z}_m^{n+1}|||^2 + (1-\alpha)\frac{\Delta t}{2}\|A_R\mathbf{z}_m^{n+1}\|^2_{L^2(\Omega)} \leq \frac{\Delta t}{2}|p_0^{n+1}|^2 + \frac{\rho}{2}|||\mathbf{u}^n|||^2 \leq \frac{\alpha^2\eta^3}{8c_1\rho}.$$

As $\eta\|\nabla\mathbf{z}_m^{n+1}\|^2_{L^2(\Omega)} \leq |||\mathbf{z}_m^{n+1}|||^2$ we deduce that $\mathbf{z}_m^{n+1}$ belongs to B_α. Thus, Brouwer's fixed point theorem can be applied: if the data are sufficiently small, i.e. (40) is satisfied, Scheme 5 has a solution $\mathbf{u}_m^{n+1}$ which belongs to B_α. This solution satisfies moreover

$$\frac{\rho}{2}|||\mathbf{u}_m^{n+1}|||^2 + (1-\alpha)\frac{\Delta t}{2}\|A_R\mathbf{u}_m^{n+1}\|^2_{L^2(\Omega)} \leq \frac{\Delta t}{2}|p_0^{n+1}|^2 + \frac{\rho}{2}|||\mathbf{u}^n|||^2.$$

Next by a compactness argument, we can pass to the limit (up to a subsequence) as m goes to infinity and there is at least a subsequence of the Galerkin approximation $(\mathbf{u}_m^{n+1})_{m\in\mathbb{N}}$ converging to $\mathbf{u}^{n+1}$ solution of Scheme 4. The *a priori* estimates obtained for $\mathbf{u}_m^{n+1}$ are inherited by this limit:

$$\frac{\rho}{2}|||\mathbf{u}^{n+1}|||^2+(1-\alpha)\frac{\Delta t}{2}\|A_R\mathbf{u}^{n+1}\|_{L^2(\Omega)}^2\leq\frac{\Delta t}{2}|p_0^{n+1}|^2+\frac{\rho}{2}|||\mathbf{u}^n|||^2. \tag{43}$$

To sum up, for a fixed n, if (40) is satisfied, there exists at least a solution $\mathbf{u}^{n+1}$ of Scheme 4 in B_α and which satisfies (43). Now we proceed by induction: if the condition (37) on the data is satisfied, assumption (40) will also be true at rank $n+1$. Moreover by summing up (43) the sequence satisfies (39).

□

Remark 11. *One could have considered another linerarization of the convection term by considering* $\rho\Delta t\left((\mathbf{w}\cdot\nabla)\mathbf{z}_m^{n+1},\mathbf{v}\right)_\Omega$ *instead of* $\rho\Delta t\left((\mathbf{z}_m^{n+1}\cdot\nabla)\mathbf{w},\mathbf{v}\right)_\Omega$. *In this case* (42) *has to be replaced by*

$$\begin{aligned}\left|\rho\Delta t\left((\mathbf{w}\cdot\nabla)\mathbf{z}_m^{n+1},A_R\mathbf{z}_m^{n+1}\right)_\Omega\right| &\leq\rho\Delta t\|\mathbf{w}\|_{L^6(\Omega)}\|\nabla\mathbf{z}_m^{n+1}\|_{L^3(\Omega)}\|A_R\mathbf{z}_m^{n+1}\|_{L^2(\Omega)}\\ &\leq c(\eta)\rho\Delta t\|\nabla\mathbf{w}\|_{L^2(\Omega)}\|A_R\mathbf{z}_m^{n+1}\|_{L^2(\Omega)}^2,\end{aligned}$$

thanks to Sobolev injections and the fact that $\mathcal{D}(A_R)$ *is continously embedded in* $\mathbf{H}^{3/2+\varepsilon}(\Omega)$ *which is itself continously embedded in* $\mathbf{W}^{1,3}(\Omega)$ *in 3D.*

Remark 12. *In Theorem 7, an implicit scheme for the convective term (i.e.* $(\mathbf{u}^{n+1}\cdot\nabla)\mathbf{u}^{n+1}$*) has been considered. Nevertheless, thanks to the previous remark, the semi-implicit treatment of convective term defined by* $(\mathbf{u}^n\cdot\nabla)\mathbf{u}^{n+1}$ *leads to the very same result (without having to apply Brouwer's fixed point Theorem).*

We now consider the uniqueness issue.

Theorem 8 (Uniqueness)**.** *Assuming that initial and boundary data are small enough, Scheme 4 has a unique solution for all* $1\leq n\leq N$.

Proof. Let us consider two solutions $\mathbf{u}_1^{n+1}$ and $\mathbf{u}_2^{n+1}$ of Scheme 4 associated to the data $p_{0,i}^{n+1}$, $i=1,2$ and to the same initial data $\mathbf{u}^0$: for $i=1,2$,

$$\begin{aligned}&\frac{\rho}{\Delta t}\int_\Omega\mathbf{u}_i^{n+1}\cdot\mathbf{v}+\rho\int_\Omega(\mathbf{u}_i^{n+1}\cdot\nabla)\mathbf{u}_i^{n+1}\cdot\mathbf{v}+\eta\int_\Omega\nabla\mathbf{u}_i^{n+1}:\nabla\mathbf{v}+R\left(\int_{\Gamma_1}\mathbf{u}_i^{n+1}\cdot\mathbf{n}\right)\left(\int_{\Gamma_1}\mathbf{v}\cdot\mathbf{n}\right)\\ &\qquad=\frac{\rho}{\Delta t}\int_\Omega\mathbf{u}^n\cdot\mathbf{v}-\int_{\Gamma_0}p_{0,i}^{n+1}\mathbf{v}\cdot\mathbf{n}.\end{aligned}\tag{44}$$

Setting $\mathbf{w}^{n+1}=\mathbf{u}_1^{n+1}-\mathbf{u}_2^{n+1}$ and $\delta p_0^{n+1}=p_{0,1}^{n+1}-p_{0,2}^{n+1}$, subtracting the two previous equations and taking $\mathbf{v}=\mathbf{w}^{n+1}$ as a test function, we obtain:

$$\begin{aligned}&\frac{\rho}{2}\|\mathbf{w}^{n+1}\|_{L^2(\Omega)}^2+\rho\Delta t\left(\mathbf{u}_1^{n+1}\cdot\nabla\mathbf{u}_1^{n+1},\mathbf{w}^{n+1}\right)_\Omega-\rho\Delta t\left(\mathbf{u}_2^{n+1}\cdot\nabla\mathbf{u}_2^{n+1},\mathbf{w}^{n+1}\right)_\Omega\\ &+\Delta t\frac{\eta}{2}\|\nabla\mathbf{w}^{n+1}\|_{L^2(\Omega)}^2+R\Delta t\left(\int_{\Gamma_1}\mathbf{w}^{n+1}\cdot\mathbf{n}\right)^2\leq\frac{\rho}{2}\|\mathbf{w}^n\|_{L^2(\Omega)}^2+\frac{\Delta t}{2}|\delta p_0^{n+1}|^2.\end{aligned}$$

We have

$$\begin{aligned}&\left(\mathbf{u}_1^{n+1}\cdot\nabla\mathbf{u}_1^{n+1},\mathbf{w}^{n+1}\right)_\Omega-\left(\mathbf{u}_2^{n+1}\cdot\nabla\mathbf{u}_2^{n+1},\mathbf{w}^{n+1}\right)_\Omega\\ &=\left(\mathbf{u}_2^{n+1}\cdot\nabla\mathbf{w}^{n+1},\mathbf{w}^{n+1}\right)_\Omega+\left(\mathbf{w}^{n+1}\cdot\nabla\mathbf{u}_2^{n+1},\mathbf{w}^{n+1}\right)_\Omega+\left(\mathbf{w}^{n+1}\cdot\nabla\mathbf{w}^{n+1},\mathbf{w}^{n+1}\right)_\Omega.\end{aligned}$$

and

$$\left|\left(\mathbf{u}_2^{n+1}\cdot\nabla\mathbf{w}^{n+1},\mathbf{w}^{n+1}\right)_\Omega\right|\leq\|\mathbf{u}_2^{n+1}\|_{L^\infty(\Omega)}\|\nabla\mathbf{w}^{n+1}\|_{L^2(\Omega)}\|\mathbf{w}^{n+1}\|_{L^2(\Omega)}.$$

Besides, thanks to Hölder inequality,

$$\left|\left(\mathbf{w}^{n+1}\cdot\nabla\mathbf{u}_2^{n+1},\mathbf{w}^{n+1}\right)_\Omega\right|\leq\|\mathbf{w}^{n+1}\|_{L^6(\Omega)}\|\nabla\mathbf{u}_2^{n+1}\|_{L^2(\Omega)}\|\mathbf{w}^{n+1}\|_{L^3(\Omega)}$$

and

$$\left|\left(\mathbf{w}^{n+1}\cdot\nabla\mathbf{w}^{n+1},\mathbf{w}^{n+1}\right)_\Omega\right|\leq\|\mathbf{w}^{n+1}\|_{L^6(\Omega)}\|\nabla\mathbf{w}^{n+1}\|_{L^2(\Omega)}\|\mathbf{w}^{n+1}\|_{L^3(\Omega)}.$$

Now Sobolev injections for $d=2,3$ lead to

$$\|\mathbf{v}\|_{L^6(\Omega)}\leq\tilde{c}\|\nabla\mathbf{v}\|_{L^2(\Omega)}$$

and

$$\|\mathbf{v}\|_{L^3(\Omega)}\leq\tilde{c}\|\mathbf{v}\|_{L^2(\Omega)}^{1/2}\|\nabla\mathbf{v}\|_{L^2(\Omega)}^{1/2}.$$

These estimates, along with Young and Poincaré's inequalities, imply

$$\frac{\rho}{2}\|\mathbf{w}^{n+1}\|^2_{L^2(\Omega)} + \Delta t\|\nabla\mathbf{w}^{n+1}\|^2_{L^2(\Omega)}\left(\frac{\eta}{8} - \tilde{c}\rho\|\mathbf{w}^{n+1}\|^{1/2}_{L^2(\Omega)}\|\nabla\mathbf{w}^{n+1}\|^{1/2}_{L^2(\Omega)}\right) + R\Delta t\left(\int_{\Gamma_1}\mathbf{w}^{n+1}\cdot\mathbf{n}\right)^2$$
$$\leq \frac{\rho}{2}\|\mathbf{w}^{n}\|^2_{L^2(\Omega)} + \frac{\Delta t}{2}|\delta p_0^{n+1}|^2 + \tilde{c}\rho\Delta t\|\mathbf{w}^{n+1}\|^2_{L^2(\Omega)}\left(\|\mathbf{u}_2^{n+1}\|^2_{L^\infty(\Omega)} + \|\nabla\mathbf{u}_2^{n+1}\|^4_{L^2(\Omega)}\right).$$

As $\mathbf{u}_1^{n+1}$ and $\mathbf{u}_2^{n+1}$ are constructed by means of Theorem 7, both solutions are in the ball B_α defined by (38). Then, as long as the term $\left(\frac{\eta}{8} - \tilde{c}\rho\|\mathbf{w}^{n+1}\|^{1/2}_{L^2(\Omega)}\|\nabla\mathbf{w}^{n+1}\|^{1/2}_{L^2(\Omega)}\right)$ is positive (which may need to restrain the radius of the ball B_α), as $\mathbf{w}^0 = \mathbf{0}$, we have:

$$\|\mathbf{w}^{n+1}\|^2_{L^2(\Omega)}\left(\frac{\rho}{2} - \tilde{c}\rho\Delta t\left(\|\mathbf{u}_2^{n+1}\|^2_{L^\infty(\Omega)} + \|\nabla\mathbf{u}_2^{n+1}\|^4_{L^2(\Omega)}\right)\right) \leq \frac{\Delta t}{2}|\delta p_0^{n+1}|^2.$$

As $\mathcal{D}(A_R) \subset L^\infty(\Omega)$ (see Lemma 3) and thanks to the fact that $|||\mathbf{u}_2^{n+1}|||^2$ and $\tilde{c}\Delta t\|A_R\mathbf{u}_2^{n+1}\|^2_{L^2(\Omega)}$ are bounded (see (39)), the data or the time-step can be chosen small enough to ensure that the term $(\frac{\rho}{2} - \tilde{c}\Delta t(\|\mathbf{u}_2^{n+1}\|^2_{L^\infty(\Omega)} + \|\nabla\mathbf{u}_2^{n+1}\|^4_{L^2(\Omega)}))$ is positive. With $\delta p_0^{n+1} = 0$, we obtain that $\mathbf{w}^{n+1} = \mathbf{0}$ and consequently the solution is unique. This concludes the proof. □

To conclude, provided that the data are regular and small enough, we obtain a unique smooth solution.

Remark 13. *A semi-discretized system has been considered. The same type of proof cannot be applied to a fully-discretized system as the function $A_R\mathbf{u}_h^{n+1}$ may not be an admissible finite element test function.*

Remark 14. *The smallness assumption* (37) *is important even in practice, as it is observed in computations which involve large applied pressures: they may lead to instabilities* [41, 11]. *We illustrate this issue in the next section and refer to* [17] *for a review of different formulations of the Navier-Stokes equations and a series of numerical test-cases. In particular, many papers study these problems and try to find numerical strategies to overcome them. For instance, the authors of* [15] *and* [28] *use Lagrange multipliers to impose a velocity profile. The authors of* [4] *and* [21] *suggest some stabilization methods.*

Here we considered Navier-Stokes equations with a R reduced-model treated with an implicit scheme. To conclude this section we briefly underline what shall be the main differences when considering an explicit coupling or RC or RCR models treated in an implicit or explicit way.

Let us consider the semi-discretized Navier-Stokes system explicitely coupled to the R model. The variational formulation writes:

Scheme 7 (Semi-discretized R model for the Navier-Stokes problem with explicit coupling)**.** *Let $\mathbf{u}^0 = \mathbf{u}_0 \in \mathbf{V}_{\mathrm{div}}$ be the initial data. Find $\mathbf{u}^{n+1}$ in $\mathbf{V}_{\mathrm{div}}$ such that, for all $\mathbf{v}$ in $\mathbf{V}_{\mathrm{div}}$:*

$$\begin{aligned}&\frac{\rho}{\Delta t}\int_\Omega \mathbf{u}^{n+1}\cdot\mathbf{v} + \rho\int_\Omega(\mathbf{u}^{n+1}\cdot\nabla)\mathbf{u}^{n+1}\cdot\mathbf{v} + \eta\int_\Omega\nabla\mathbf{u}^{n+1}:\nabla\mathbf{v}\\ &= \frac{\rho}{\Delta t}\int_\Omega\mathbf{u}^n\cdot\mathbf{v} - p_0^{n+1}\int_{\Gamma_0}\mathbf{v}\cdot\mathbf{n} - R\left(\int_{\Gamma_1}\mathbf{u}^n\cdot\mathbf{n}\right)\left(\int_{\Gamma_1}\mathbf{v}\cdot\mathbf{n}\right).\end{aligned} \tag{45}$$

The resulting operator is A_0, instead of A_R, and one has an additional source term to estimate that writes, by taking $\mathbf{v} = A_0\mathbf{u}^{n+1}$ as a test function: $R\left(\int_{\Gamma_1}\mathbf{u}^n\cdot\mathbf{n}\right)\left(\int_{\Gamma_1}A_0\mathbf{u}^{n+1}\cdot\mathbf{n}\right)$. Using Lemma 1 we obtain the following bound

$$\begin{aligned}\left|R\left(\int_{\Gamma_1}\mathbf{u}^n\cdot\mathbf{n}\right)\left(\int_{\Gamma_1}A_0\mathbf{u}^{n+1}\cdot\mathbf{n}\right)\right| &\leq R\|\mathbf{u}^n\|_{L^2(\Omega)}\|A_0\mathbf{u}^{n+1}\|_{L^2(\Omega)}\\ &\leq 2R^2\|\mathbf{u}^n\|^2_{L^2(\Omega)} + \frac{1}{4}\|A_0\mathbf{u}^{n+1}\|^2_{L^2(\Omega)}\\ &\leq 2\frac{R^2}{\eta}|||\mathbf{u}^n|||^2_{L^2(\Omega)} + \frac{1}{4}\|A_0\mathbf{u}^{n+1}\|^2_{L^2(\Omega)},\end{aligned}$$

where $|||\cdot|||$ is now the norm associated to A_0. Thanks to this estimate, if we follow the same lines as in the proof of Theorem 7, assumption (40) has to be replaced by a more restrictive one:

$$\frac{\Delta t}{2}|p_0^{n+1}|^2 + \left(\frac{\rho}{2} + 2\Delta t\frac{R^2}{\eta}\right)|||\mathbf{u}^n|||^2 \leq \frac{\alpha^2\eta^3}{16c_1\rho}, \tag{46}$$

which leads, by applying a discrete Gronwall lemma, to the following condition on the data

$$\exp\left(\tilde{c}\frac{R^2}{\rho\eta}T\right)\left(\frac{\rho}{2}|||\mathbf{u}^0|||^2 + \frac{\Delta t}{2}\sum_{k=1}^N|p_0^k|^2\right) \leq \frac{\alpha^2\eta^3}{16c_1\rho}. \tag{47}$$

Note that this new condition involves not only the initial velocity and the applied pressure but also the final time T together with the same exponential growth as in *Result 1* of Theorem 2. Under assumption (47), we

		Blood	Air	He-O_2
Density	$(\mathrm{g}\cdot\mathrm{cm}^{-3})$	$1.06\cdot 10^{+0}$	$1.20\cdot 10^{-3}$	$1.80\cdot 10^{-4}$
Viscosity	$(\mathrm{g}\cdot\mathrm{cm}^{-1}\cdot\mathrm{s}^{-1})$	$4.00\cdot 10^{-2}$	$2.00\cdot 10^{-4}$	$2.00\cdot 10^{-4}$

TABLE 1. Density and viscosity for blood, air and helium-oxygen mixture (He-O_2).

obtain the existence of at least one strong solution as well as a stability estimate without CFL like condition but under strong smallness assumptions on the data. We can asset that this sufficient condition may be worse when dealing with more general reduced models such as RC or RCR models. Without going into details we now underline what would be the major difficulties if we consider these RC or RCR models. The first remark is that the choice of the operator "A" depends on the considered case: $A_{\frac{RC+\Delta t}{C}}$ for the RC model with an implicit coupling, A_{R_p} for the RCR model with an implicit coupling and A_0 in any case for the explicit schemes. The second remark is that even with an implicit coupling the analysis differs a lot from the one performed for the Stokes system or from the Navier-Stokes system with implicit coupling with the R model. Indeed some terms involving products of integrals such as $\left(\int_{\Gamma_1}\mathbf{u}^k\cdot\mathbf{n}\right)\left(\int_{\Gamma_1}A\mathbf{u}^{n+1}\cdot\mathbf{n}\right)$ will have to be estimated even if we make an appropriate choice of the operator A. Consequently one can expect that the existence and stability results would follow the same lines as for the Stokes system with RC or RCR models with an explicit coupling (for which residual products of fluxes have to be estimated) and thus lead to some requirement of CFL-like conditions and smallness of the data.

5. Scientific computing: numerical stability observations

This section aims at illustrating and discussing some of the theoretical results obtained in the previous sections but also at performing some realistic simulations in the context of blood flows and airflows. Computations have been performed with the software Felisce [14], which is a parallel finite element code written in `C++`. FELiScE stands for "Finite Elements for LIfe SCiences and Engineering".

5.1. Preliminaries: data, parameters, notations.

In all the simulations, we use the CGS units: centimetres (cm), grams (g) and seconds (s). Then the fluxes are expressed in $\mathrm{cm}^3\cdot\mathrm{s}^{-1}$, and pressures in barye (ba). We note that $1\,\mathrm{ba} = 0.1\,\mathrm{Pa}$. We use physiological parameters detailed in Table 1. In CGS units, resistance R is expressed in $\mathrm{g}\cdot\mathrm{cm}^{-4}\cdot\mathrm{s}^{-1}$ and compliance C is expressed in $\mathrm{g}^{-1}\cdot\mathrm{cm}^4\cdot\mathrm{s}^2$.

For each test-case, we define a *reference solution* as the solution computed with a fine mesh and a time-step small enough in order to obtain converged solutions. The linear systems resulting from the time-space discretization are solved with a generalized minimal residual method (GMRES). To characterize the convergence and the stability of each computation, we use the following symbols:

(1) ■ the convergence failed in the linear solver. Then the linear system cannot be solved and the computation stops before the final time, see Figure 4(e), page 7.
(2) ⊠ the GMRES algorithm converges at each time-step but the solution is unstable, see Figure 4(a), page 7.
(3) ⊕ the GMRES algorithm converges at each time-step and the scheme is stable, but spurious oscillations are observed around the reference solution, see Figure 4(b), page 7.
(4) ◯ the GMRES algorithm has converged at each time-step and the scheme is stable, with a solution in good agreement with the reference solution, see Figure 4(c), page 7.

A restarted GMRES algorithm is used to solve the linear systems. The method is restarted after 200 iterations. We use a relative tolerance of 10^{-8} and an absolute one of 10^{-10}. The maximum number of iterations is 10 000 and the solver is initialized with the previous solution. Note that if the used tolerances are not small enough, oscillations linked to the lack of precision of the iterative method may appear.

5.2. Stokes flow in a tube geometry.

In this subsection, we aim at illustrating some results obtained in Section 3 on the Stokes system. We consider the Stokes equations in a tube with a sinusoidal applied pressure at the inlet and reduced models coupled at the outlet. We compare stability properties for different physical parameters (resistance R, density ρ, viscosity η and, possibly, compliance C) and different discretization parameters (time-step Δt and mesh size h), using explicit or implicit coupling schemes. A Galerkin method with $\mathbb{P}2/\mathbb{P}1$ finite elements is considered, and we use tube meshes described in Table 2.

Let us first consider the Stokes system coupled with the R model and solved by the explicit scheme. In Figures 5 and 6, we observe that, for a given time step, increasing the resistance or decreasing the density leads to numerical instabilities. This suggests the existence of a CFL condition that could be related to condition (11).

The Stokes system coupled with the RCR model behaves as the R model, as Theorem 6 is similar to Theorem 2.

The Stokes system coupled with the RC model is solved by the explicit scheme. Figure 9 illustrates condition (25): the smaller the compliance is, the more we observe numerical instabilities. Note that in the considered

Name of the mesh	$N_{\text{th.}}$	$N_{\text{tr.}}$	DOF($\mathbf{u}$)	DOF(p)	h
Coarse	9 954	1 922	45 900	2 193	0.09
Fine	192 560	19 980	830 091	37 074	0.06

TABLE 2. Main characteristics of the tube meshes used in the simulations with a $\mathbb{P}2/\mathbb{P}1$ approximation: $N_{\text{th.}}$ denotes the number of tetrahedra, $N_{\text{tr.}}$ the number of triangles (boundary elements), DOF($\mathbf{u}$) the number of degrees of freedom for the velocity field, DOF(p) the number of degrees of freedom for the pressure field and h is the mesh size.

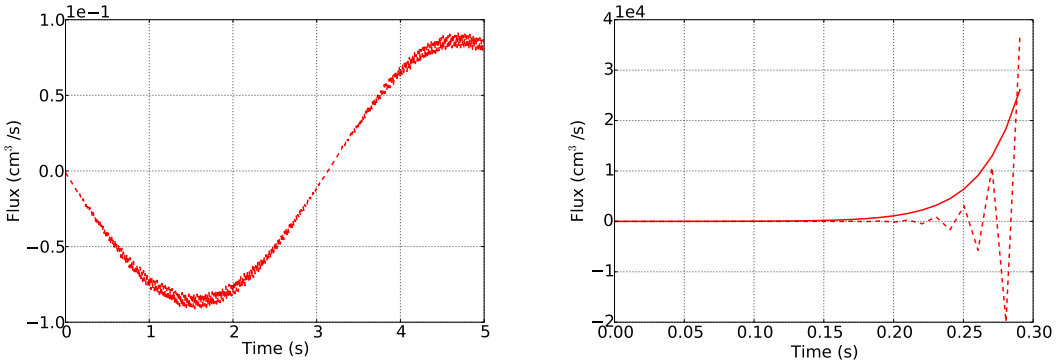

FIGURE 5. *Explicit scheme applied to the Stokes system with R model.* Flow over time at the entrance of the tube with $\Delta t = 10^{-2}$ and $p_{\text{in}}^{n+1}(t) = \sin(t^{n+1})$ for $R = 10$ (left) and $R = 20$ (right), $\rho = 1.2.10^{-3}$, $\eta = 2.10^{-4}$, CGS units, with the coarse mesh. On the right, the solid line represents an exponential growth.

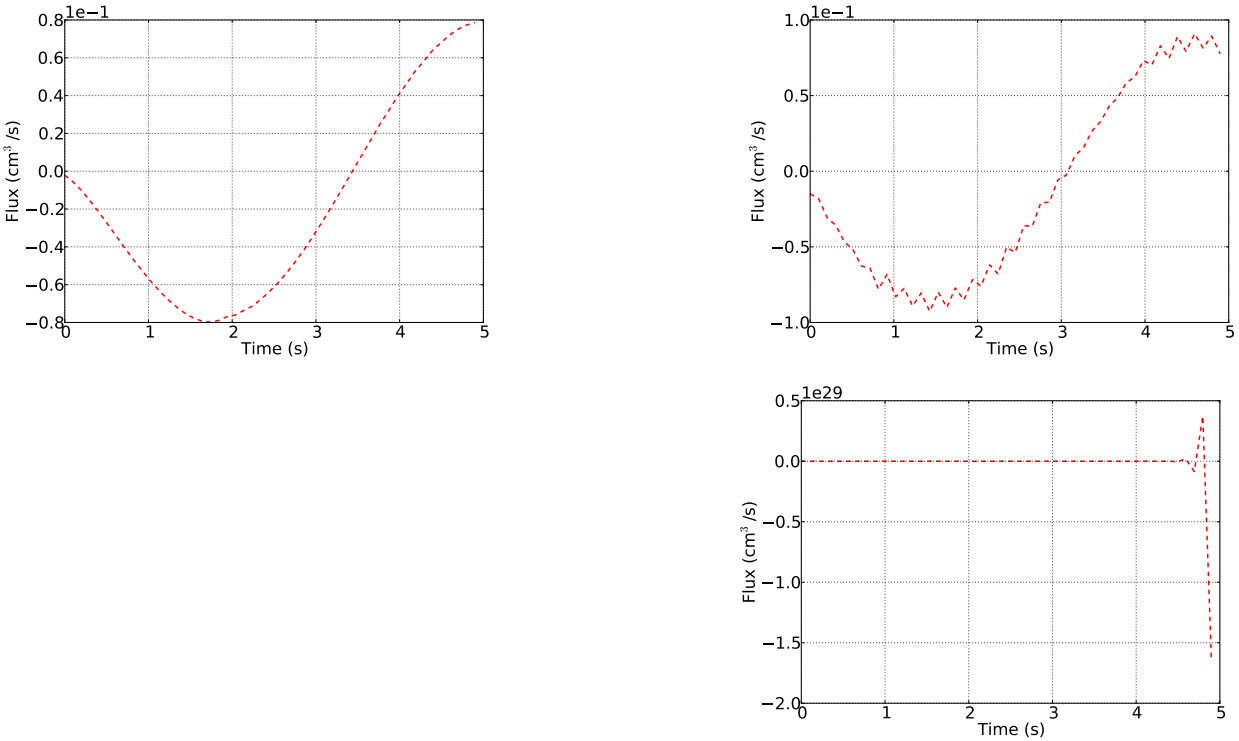

FIGURE 6. *Explicit scheme applied to the Stokes system with R model.* Flow over time at the entrance of the tube with $\Delta t = 10^{-1}$ and $p_{\text{in}}^{n+1}(t) = \sin(t^{n+1})$ for $\rho = 0.1$ (left), $\rho = 0.01$ (center) and $\rho = 0.001$ (right), $\eta = 2.10^{-4}$, CGS units, with the coarse mesh.

test-case, we did not observe any stability limitation with respect to the final time T, unlike what is suggested by condition (25).

In the same geometry we now investigate the influence of the physiological parameters (corresponding to airflows and blood flows) by computing the Stokes flow with R model. Here we choose $R = 100$, $p_{\text{in}}(t) = 1.0{\cdot}\sin(t)$ and various physiological parameters that model blood, air and helium-oxygen mixture characteristics, see

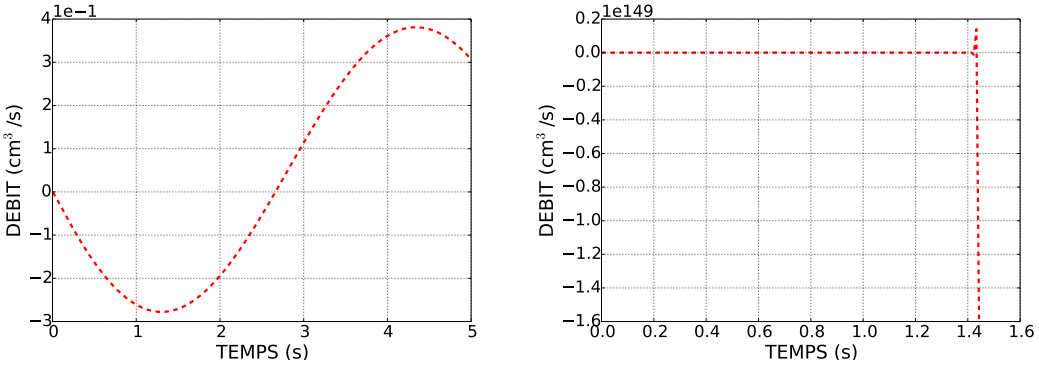

FIGURE 7. *Explicit scheme applied to the Stokes system with RC model.* Flow over time at the entrance of the tube with $\Delta t = 1.0 \cdot 10^{-2}$ and $p_{\text{in}}^{n+1}(t) = \sin(t^{n+1})$, $R = 1.0$, $C = 1.0$ (left) and $C = 1.0 \cdot 10^{-4}$ (right), $\rho = 1.2.10^{-3}$, $\eta = 2.10^{-4}$, CGS units, with the coarse mesh.

	Blood	Air	He-O_2
R	$1.00 \cdot 10^{+2}$	$1.00 \cdot 10^{+2}$	$1.00 \cdot 10^{+2}$
ρ	$1.06 \cdot 10^{+0}$	$1.20 \cdot 10^{-3}$	$1.80 \cdot 10^{-4}$

TABLE 3. Physical parameters, in CGS units.

Mesh	h	Explicit coupling scheme			
		Δt	Blood	Air	He-O_2
Coarse	0.09	10^{-2}	○	■	■
		10^{-3}	○	○	■
		10^{-4}	○	○	○
Fine	0.06	Δt	Blood	Air	He-O_2
		10^{-2}	○	■	■
		10^{-3}	○	○	■
		10^{-4}	○	○	○
Mesh	h	Implicit coupling scheme			
		Δt	Blood	Air	He-O_2
Coarse	0.09	10^{-2}	○	○	○
		10^{-3}	○	○	○
		10^{-4}	○	○	○
Fine	0.06	Δt	Blood	Air	He-O_2
		10^{-2}	○	○	○
		10^{-3}	○	○	○
		10^{-4}	○	○	○

TABLE 4. *Stokes system with R model.* Comparison of stability results for various fluids in a tube.

Table 3. Note that ρ/R is smaller in airflows than blood flows and it is even smaller in the case of an helium-oxygen mixture.

Table 4 reports the related test-cases in which we consider different time steps, explicit or implicit coupling for two types of meshes. As observed previously, a CFL condition seems to be necessary to ensure stability of the computations in the explicit case.

Remark 15. *The implicit scheme for the reduced models implies changes in the pattern of the linear system matrix. Considering this implicit scheme and larger tolerance parameters for the iterative method (a relative tolerance equal to* 10^{-6} *and an absolute one equal to* 10^{-8}*) leads to some oscillations, in particular with the finer mesh. However, we show that this scheme is unconditionally stable, see Section 3. Computing these test-cases with lower tolerance parameters, these unsuitable behaviours disappear. Consequently, these instabilities are linked to the iterative method used to solve the linear system. We observed that the smaller the h parameter is, the larger the needed GMRES precision is. We also observe that the smaller the density is, the larger the needed GMRES precision is. To finish, computing the same test-cases with smaller R parameter, we note that the larger the resistance is, the larger the needed GMRES precision is.*

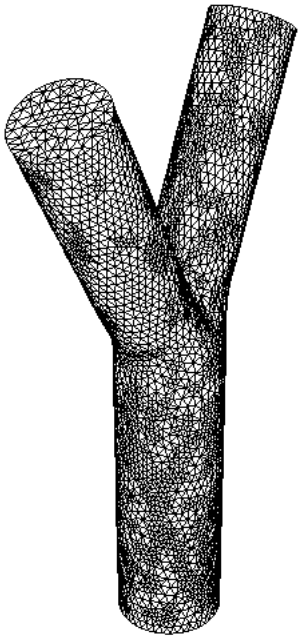

FIGURE 8. Bifurcation mesh

Name of the mesh	$N_{\text{th.}}$	$N_{\text{tr.}}$	DOF($\mathbf{u}$)	DOF(p)	h
Coarse	5 354	1 286	25 494	1 251	0.31
Fine	308 689	29 994	1 324 017	58 827	0.09

TABLE 5. Main characteristics of the bifurcation meshes used in the simulations with a $\mathbb{P}2/\mathbb{P}1$ approximation: $N_{\text{th.}}$ denotes the number of tetrahedra, $N_{\text{tr.}}$ the number of triangles (boundary elements), DOF($\mathbf{u}$) the number of degrees of freedom for the velocity field, DOF(p) the number of degrees of freedom for the pressure field and h is the mesh size.

R_1, R_2	C_1, C_2	A_{in}
$1.53 \cdot 10^{+0}$	$9.40 \cdot 10^{-3}$	$2.60 \cdot 10^{+3}$

TABLE 6. Parameters used in the simulations for the respiratory tract. Here A_{in} denotes the amplitude of the pressure at the entrance: $p_{\text{in}}(t) = A_{\text{in}} \sin(t)$. CGS units.

Remark 16. *When computing all the test-cases presented in Table 4 with free outlet boundary condition ($\eta\nabla\mathbf{u}\cdot\mathbf{n} - p\mathbf{n} = 0$), we do not observe any oscillation. Thus the observed instabilities in Table 4 come from the reduced models.*

5.3. **Stokes flow in a bifurcation geometry.** In this subsection, we consider a more complex geometry: a bifurcation. We investigate the numerical stability of the coupling between the 3D model and 0D reduced ones with parameters that reproduce physiological flows: a RCR model for blood and a RC model for air and helium-oxygen mixture, see Subsection 2.2. Inlet applied pressures are also adapted to each application to get the same flow regime as in real cases. In the simulations, two bifurcation meshes are used, see Figure 8 and Table 5: a coarse mesh and a fine mesh, and $\mathbb{P}2/\mathbb{P}1$ finite elements are used.

In order to model physiological flows, we choose parameters as described in Table 6 for airflows and Table 7 for blood flows.

In Table 8, once again, in the explicit case, numerical instabilities are observed for helium-oxygen mixtures whereas this trend vanishes when considering air and blood. Nevertheless, decreasing the time step makes the explicit coupling scheme stable as is the implicit coupling scheme.

5.4. **Navier-Stokes flow in a bifurcation geometry: the stabilization issue.** In this subsection, we show how numerical instabilities may occur when considering the Navier-Stokes system with Neumann boundary

$R_{p,1}, R_{p,2}$	C_1, C_2	$R_{d,1}, R_{d,2}$	$P_d(t=0)$	A_{in}
$1.00 \cdot 10^{+3}$	$1.00 \cdot 10^{-4}$	$1.00 \cdot 10^{+4}$	$1.00 \cdot 10^{+5}$	$8.00 \cdot 10^{+4}$

TABLE 7. Parameters used in the simulations for the aorta. Here A_{in} denotes the amplitude of the pressure at the entrance: $p_{in}(t) = A_{in}\sin(t)$. CGS units.

Mesh	h	Explicit coupling scheme			
		Δt	Blood	Air	He-O_2
Coarse	0.31	10^{-2}	◯	⊠	■
		10^{-3}	◯	◯	◯
		10^{-4}	◯	◯	◯
		Δt	Blood	Air	He-O_2
Fine	0.09	10^{-2}	◯	⊠	■
		10^{-3}	◯	◯	◯
		10^{-4}	◯	◯	◯
Mesh	h	Implicit coupling scheme			
		Δt	Blood	Air	He-O_2
Coarse	0.31	10^{-2}	◯	◯	◯
		10^{-3}	◯	◯	◯
		10^{-4}	◯	◯	◯
		Δt	Blood	Air	He-O_2
Fine	0.09	10^{-2}	◯	◯	◯
		10^{-3}	◯	◯	◯
		10^{-4}	◯	◯	◯

TABLE 8. *Stokes system in a bifurcation.* RC model for respiratory flows (air or He-O_2) and RCR model for blood flows.

conditions, namely $R = 0$. We aim at illustrating the theoretical results stated in Theorem 7 and the intrinsic drawback related to the amount of kinetic energy entering the 3D domain because of the artificial boundaries in the Navier-Stokes system.

Figure 9 exhibits the typical numerical behaviour at the inlet that emerges from the lack of energy estimate and appears as soon as the data are large enough.

Since we aim at simulating flows in realistic and physiological conditions for which inertial effects have to be taken into account, here we choose to use numerical strategies in order to overcome the instabilities due to possible incoming kinetic energy. In the context of physiological flows, many strategies have been proposed in the past: the velocity profile can be prescribed as in [15, 28]; alternatively, various stabilization methods have been introduced, see [4, 21], leading to the modification of the resulting physical system. We refer to [17] for a review on these questions. In what follows, we choose to solve the Navier-Stokes system with a semi-implicit treatment of the convective term (with the following discretization in time: $\mathbf{u}^n \cdot \nabla \mathbf{u}^{n+1}$) and, then, stabilize the system by adding to the normal constraint in the variational formulation the following term:

$$-\beta \frac{\rho}{2} \int_{\Gamma_1} (\mathbf{u}^n \cdot \mathbf{n})_- (\mathbf{u}^{n+1} \cdot \mathbf{v}), \quad \beta \in (0,1], \tag{48}$$

where $(\mathbf{u}^n \cdot \mathbf{n})_-$ is defined as

$$(\mathbf{u}^n \cdot \mathbf{n})_- = \frac{\mathbf{u}^n \cdot \mathbf{n} - |\mathbf{u}^n \cdot \mathbf{n}|}{2} = \begin{cases} \mathbf{u}^n \cdot \mathbf{n} & \text{if } \mathbf{u}^n \cdot \mathbf{n} < 0, \\ 0 & \text{otherwise.} \end{cases}$$

This procedure, we will refer to as stabilization method, has been introduced in [7] for $\beta = 1$ and used in the context of blood flows for instance in [4, 21]. For $\beta = 1$, it ensures that the solution of the system satisfies energy estimates and, from the physical point of view, traduces the fact that it costs energy to make the fluid enter the domain. Indeed the added term is an outward traction, opposite the direction of backflow, which pushes the flow in the direction of the outward normal. This term provides the missing convective flow information from outside of the computational domain during flow reversal. We will use this backflow stabilization strategy with $\beta = 1$ in our numerical simulations for realistic tests-cases. Note that when $\beta \neq 1$ no energy bound are available, leading to the same stabilities issues as for the Navier-Stokes system. In practice β is then chosen to control the amount of kinetic energy entering the computational domain.

5.5. **Physiological flows in realistic geometries.** In this subsection, we simulate physiological flows for both applications: flows of air or helium-oxygen mixtures in the respiratory tract and blood flow in the aorta. Real

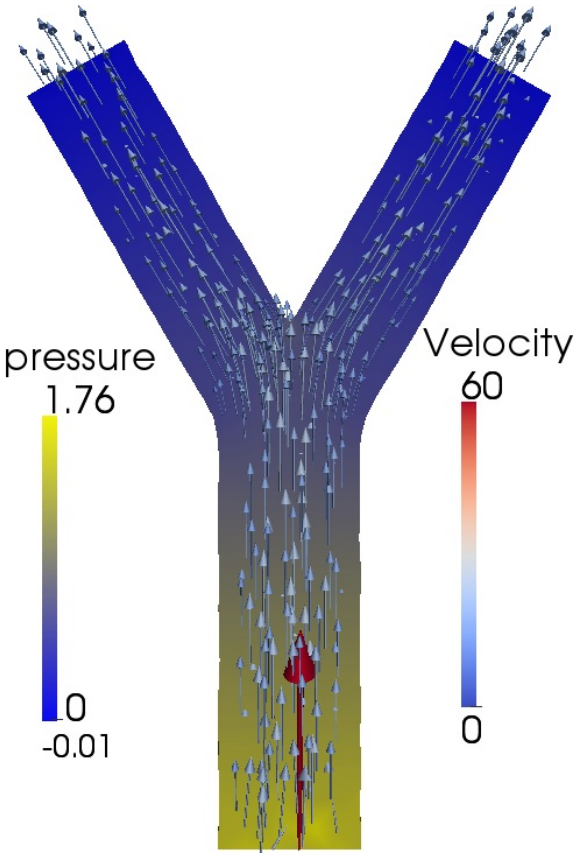

FIGURE 9. Example of numerical instability emerging from the lack energy estimate the Navier-Stokes system with Neumann boundary conditions in a 3D bifurcation

Name of the mesh	$N_{\text{th.}}$	$N_{\text{tr.}}$	DOF($\mathbf{u}$)	DOF(p)	h
respiratory tract	510 382	48 694	292 011	97 337	0.32
aorta	126 200	13 564	73 164	24 388	0.32

TABLE 9. Main characteristics of the meshes for realistic geometries, used in the simulations with a stabilized $\mathbb{P}1/\mathbb{P}1$ approximation: $N_{\text{th.}}$ denotes the number of tetrahedra, $N_{\text{tr.}}$ the number of triangles (boundary elements), DOF($\mathbf{u}$) the number of degrees of freedom for the velocity field, DOF(p) the number of degrees of freedom for the pressure field and h is the mesh size.

or realistic geometries of human proximal bronchial tree or human aorta are used, and we compare stability properties for blood, air and helium-oxygen mixture, with applied pressure and reduced model adapted to each case, with explicit or implicit coupling schemes.

As outlined above, we consider here the wall of the two geometries as rigid, which is a strong hypothesis. The following comparison may be different considering fluid-structure interaction due to the wall motion.

In the following test-cases, a bronchial tree and an idealized aorta are used. We gather the characteristics of the meshes in Table 9. Note that the mesh size is the same in both geometries. Here due to the large number of degree of freedom we use a stabilized $\mathbb{P}1/\mathbb{P}1$ finite element approximation. Moreover, as already mentioned, we stabilized the backflow phenemena by adding the term defined by (48) to the variational formulation.

For the blood test-cases, $p_{\text{in}}(t) = A_{\text{in}} \sin(t)$ with $A_{\text{in}} = 8.0 \cdot 10^{+4}$ is applied at the inlet. The physical parameters used for each RCR model coupled to the four outlet are described in Table 10. Moreover, each distal pressure is initialized at $1.0 \cdot 10^{+5}$.

For the air and helium-oxygen mixture test-cases, a pressure $p_{\text{in}}(t) = A_{\text{in}} \sin(t)$ with $A_{\text{in}} = 2.6 \cdot 10^{+3}$ is applied at the inlet. The resistance values are chosen using anatomical data from [43], assuming that each outlet i is connected to a dyadic subtree where the flow is assumed non-inertial, i.e. with a low Reynolds number and thus characterized by a resistance R_i depending on the generation j at which the artificial boundary is located.

To parametrize the compliance of each RC reduced model coupled at each outlet of the bronchial tree, we suppose that the first generations (i.e. the three-dimensional part) are rigid and we choose to split the compliance of the whole human lung tissues (around 0.2 L/mmHg $\sim 0.15\,\text{g}^{-1} \cdot \text{cm}^4 \cdot \text{s}^2$ [3, 5, 44, 23]) between all

Outlet	R_{p}	C	R_{d}
outlet at the top n^o 1	$5.00 \cdot 10^{+2}$	$9.50 \cdot 10^{-5}$	$8.50 \cdot 10^{+3}$
outlet at the top n^o 2	$1.90 \cdot 10^{+3}$	$2.50 \cdot 10^{-5}$	$3.22 \cdot 10^{+4}$
outlet at the top n^o 3	$7.50 \cdot 10^{+2}$	$6.40 \cdot 10^{-5}$	$1.25 \cdot 10^{+4}$
outlet at the bottom	$1.50 \cdot 10^{+2}$	$3.17 \cdot 10^{-4}$	$2.50 \cdot 10^{+3}$

TABLE 10. Parameters used in the simulations for the aorta. CGS units.

3D/0D interface generation j	R_j	C_j	3D mesh
1	$1.30 \cdot 10^{-1}$	$1.50 \cdot 10^{-1}$	Tube
2	$2.40 \cdot 10^{-1}$	$7.50 \cdot 10^{-2}$	Bifurcation
3	$4.60 \cdot 10^{-1}$	$3.70 \cdot 10^{-2}$	
4	$8.40 \cdot 10^{-1}$	$1.90 \cdot 10^{-2}$	
5	$1.53 \cdot 10^{+0}$	$9.40 \cdot 10^{-3}$	

TABLE 11. Subtree resistances and compliances for different generations, taking $C_{\mathrm{total}} = 0.15\,\mathrm{g}^{-1} \cdot \mathrm{cm}^4 \cdot \mathrm{s}^2$. CGS units.

h	Explicit coupling scheme			
	Δt	Blood RCR	Air RC	He-O_2 RC
0.32	10^{-2}	⊕	■	■
	10^{-3}	○	■	■
	10^{-4}	○	■	■
h	Implicit coupling scheme			
	Δt	Blood RCR	Air RC	He-O_2 RC
0.32	10^{-2}	○	■	■
	10^{-3}	○	■	■
	10^{-4}	○	■	■

TABLE 12. Comparison of stability behaviour between blood, air and helium-oxygen mixture flows in real geometries, for Navier-Stokes system. Physiological applied pressures.

the artificial boundaries. Table 11 presents the resistance and compliance values depending on the generation j where the outlet is located.

In Figures 10 and 11, we plot the pressure and the velocity obtained solving Navier-Stokes equations in both geometries. It illustrates the abilility of the solver to perform simulations on complex geometries and in a physiological context. Next we compare the stability of various computations making the time step varies for different fluids in their associated geometry and coupled, explicitly or implicitly, to the appropriate reduced model.

Table 12 illustrates that computations with helium-oxygen mixture or air in the respiratory tract seems to be more sensitive than computations with blood in an artery even in the implicit case. In the explicit case it could be due to the fact that CFL conditions are not satisfied. Nevetheless for the bronchial tree, when decreasing the time step the computations remain unstable and the same behavior is observed for the implicit treatment. Consequenlty, these instabilities may be due to conditioning issues, to the complexity of the geometry or to the considered reduced model. Note moreover that, even if we are in a case where energy estimates are satisfied thanks to the stabilization term, considering lower applied pressure leads to less instabilities, see Table 13. In this case the explicit scheme and the implicit scheme behave in a similar way.

6. CONCLUSION

To conclude, in this paper, we investigated stability issues link to the Navier-Stokes system in a truncated domain and its coupling with different 0D reduced models. The considered numerical strategies to advance in time the associated linear 3D/0D coupled system lead to unconditionally stable schemes in the implicit case and possibly conditionally stable schemes in the explicit one. The obtained CFL conditions depend on the fluid properties together with the considered 0D model. Note that, when considering the implicit treatment, it may lead to conditioning issues implying costly and not even converged computations. One way to avoid these conditioning issues is, for instance, to use the method introduced in [10]. Furthermore if the implicit coupling is

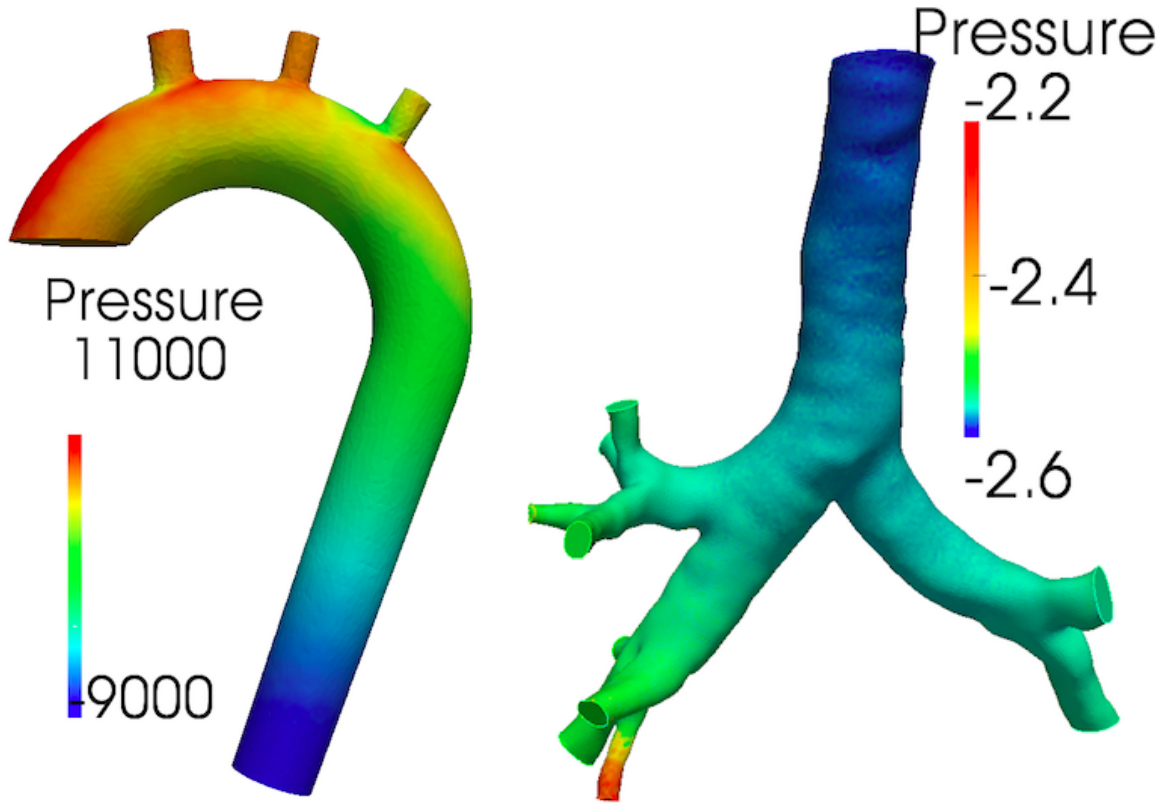

FIGURE 10. Pressure (in barye, i.e. 0.1 Pascal) at time $t = 0.1$ solving Navier-Stokes equations with stabilized $\mathbb{P}1/\mathbb{P}1$ finite elements and backflow stabilization (see (48)).

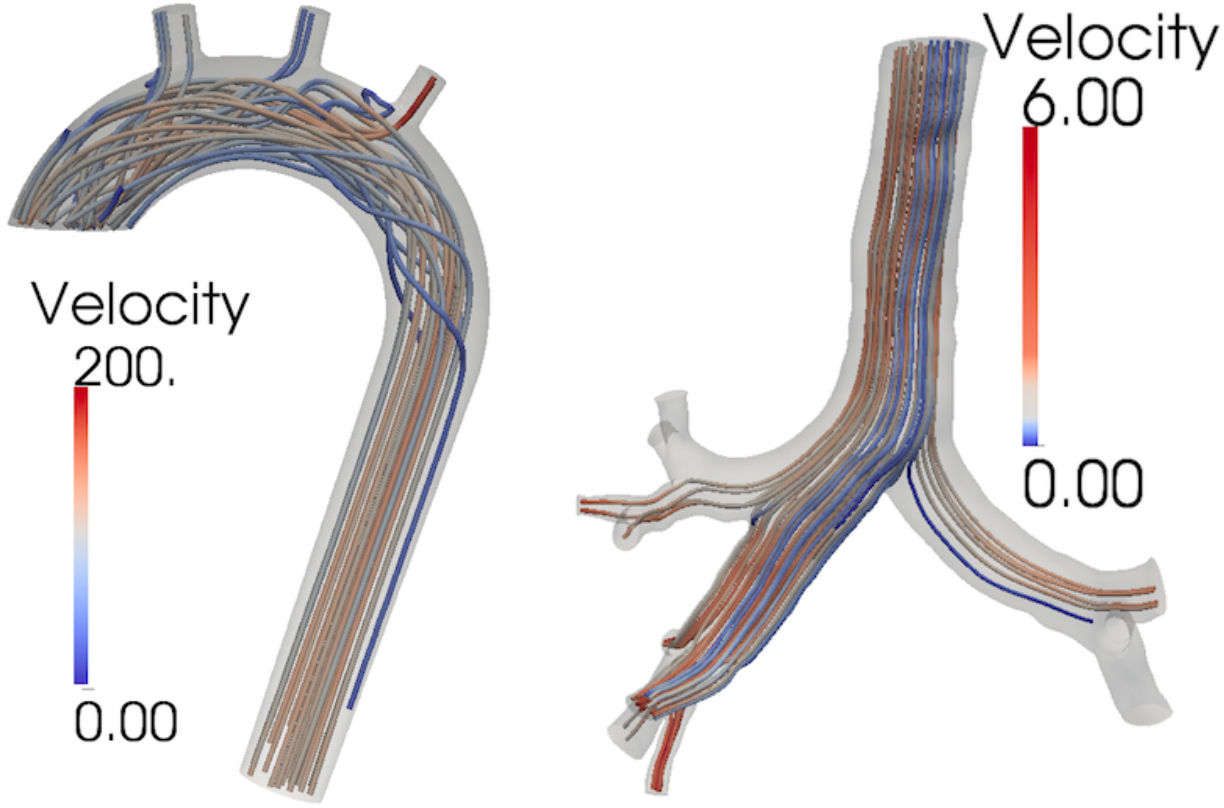

FIGURE 11. Velocity (in $\mathrm{cm}\cdot\mathrm{s}^{-1}$) at time $t = 0.1$ solving Navier-Stokes equations with stabilized $\mathbb{P}1/\mathbb{P}1$ finite elements and backflow stabilization (see (48)).

h	Explicit coupling scheme			
	Δt	Blood RCR	Air RC	He-O_2 RC
0.32	10^{-2}	⊕	■	■
	10^{-3}	○	⊠	■
	10^{-4}	○	○	○
h	Implicit coupling scheme			
	Δt	Blood RCR	Air RC	He-O_2 RC
0.32	10^{-2}	○	■	■
	10^{-3}	○	⊠	■
	10^{-4}	○	○	○

TABLE 13. Comparison of stability behaviour between blood, air and helium-oxygen mixture flows in real geometries, for Navier-Stokes system. Low applied pressures.

achieved thanks to an iterative procedure, we deduce from our stability estimates that limitations on the time step may be needed which are similar from the one in the explicit case.

We also derived new estimates for the semi-discretized Navier-Stokes system coupled to 0D reduced models, under strong assumptions of smallness of the data and in particular the external applied pressure. Moreover, in this nonlinear case, even when considering an implicit coupling, the numerical stability can be subjected to CFL conditions (in particular with the RC or RCR models). It underlines the intrinsic difficulty of performing computations for the Navier-Stokes system with Neumann boundary conditions or for the Navier-Stokes system coupled to reduced models. It justifies the need to design and use appropriate and physically relevant backflow stabilization methods or to impose non standard boundary conditions (involving the total pressure for instance) to perform realistic simulations in regions where inertia effects can not be neglected.

REFERENCES

[1] J. Alastruey, K. H. Parker, J. Peiró, and S. J. Sherwin. Analysing the pattern of pulse waves in arterial networks: a time-domain study. *Journal of Engineering Mathematics*, 64(4):331–351, 2009.

[2] L. Baffico, C. Grandmont, and B. Maury. Multiscale modeling of the respiratory tract. *Mathematical Models & Methods in Applied Sciences*, 20(1):59–93, 2010.

[3] J. H. T. Bates. *Lung Mechanics: An Inverse Modeling Approach*. Cambridge University Press, 2009.

[4] Y. Bazilevs, J. R. Gohean, T. J. R. Hughes, R. D. Moser, and Y. Zhang. Patient-specific isogeometric fluid-structure interaction analysis of thoracic aortic blood flow due to implantation of the jarvik 2000 left ventricular assist device. *Computer Methods in Applied Mechanics and Engineering*, 198(45-46):3534–3550, 2009.

[5] A. Ben-Tal. Simplified models for gas exchange in the human lungs. *Journal of Theoretical Biology*, 238(2):474–495, 2006.

[6] C. Bertoglio, A. Caiazzo, and M. A. Fernández. Fractional-step schemes for the coupling of distributed and lumped models in hemodynamics. *SIAM Journal on Scientific Computing*, 35(3):B551–B575, 2013.

[7] C.-H. Bruneau and P. Fabrie. New efficient boundary conditions for incompressible Navier–Stokes equations : a well-posedness result. *ESAIM: Mathematical Modelling and Numerical Analysis - Modélisation Mathématique et Analyse Numérique*, 30(7):815–840, 1996.

[8] A. J. Chorin. Numerical solution of the Navier–Stokes equations. *Mathematics of Computation*, 22(104):745–762, 1968.

[9] A. J. Chorin. On the convergence of discrete approximations to the Navier–Stokes equations. *Math. Comp*, 23(106):341–353, 1969.

[10] A. Devys, C. Grandmont, B. Grec, B. Maury, and D. Yakoubi. Numerical method for the 2D simulation of the respiration. In *ESAIM: Proceedings*, volume 28, pages 162–181, 2009.

[11] M. Esmaily Moghadam, Y. Bazilevs, T.-Y. Hsia, I. E. Vignon-Clementel, A. L. Marsden, and Modeling of Congenital Hearts Alliance (MOCHA) Investigators. A comparison of outlet boundary treatments for prevention of backflow divergence with relevance to blood flow simulations. *Computational Mechanics*, 48(3):277–291, 2011.

[12] M. Esmaily Moghadam, F. Migliavacca, I. E. Vignon-Clementel, T.-Y. Hsia, A. Marsden, and Modeling of Congenital Hearts Alliance (MOCHA) Investigators. Optimization of shunt placement for the norwood surgery using multi-domain modeling. *Journal of Biomechanical Engineering*, 134(5):051002, 2012.

[13] M. Esmaily Moghadam, I. E. Vignon-Clementel, R. Figliola, and A. L. Marsden. A modular numerical method for implicit 0D/3D coupling in cardiovascular finite element simulations. *Journal of Computational Physics*, 244(0):63–79, 2012.

[14] FELiScE. INRIA forge project FELiScE : felisce.gforge.inria.fr. 2014.

[15] L. Formaggia, A. Moura, and F. Nobile. On the stability of the coupling of 3D and 1D fluid-structure interaction models for blood flow simulations. *ESAIM-Mathematical Modelling and Numerical Analysis*, 41(4):743–770, 2007.

[16] L. Formaggia, A. Quarteroni, and A. Veneziani. *Cardiovascular Mathematics Modeling and simulation of the circulatory system*. Springer-Verlag, Milan, 2009.

[17] J. Fouchet-Incaux. Artificial boundaries and formulations for the incompressible Navier–Stokes equations: applications to air and blood flows. *SeMA Journal*, 64(1):1–40, 2014.

[18] T. Gengenbach, V. Heuveline, and M. J. Krause. Numerical simulation of the human lung: A two-scale approach. *EMCL Preprint Series*, 11, 2011.

[19] J.-F. Gerbeau, M. Vidrascu, and P. Frey. Fluid-structure interaction in blood flows on geometries based on medical imaging. *Computers & Structures*, 83(2-3):155–165, 2005.
[20] C. Grandmont, Y. Maday, and B. Maury. A multiscale/multimodel approach of the respiration tree. In *New trends in continuum mechanics*, volume 3 of *Theta Ser. Adv. Math.*, pages 147–157. Theta, Bucharest, 2005.
[21] V. Gravemeier, A. Comerford, L. Yoshihara, M. Ismail, and W. A. Wall. A novel formulation for Neumann inflow boundary conditions in biomechanics. *International Journal for Numerical Methods in Biomedical Engineering*, 28(5):560–573, 2012.
[22] J.-L. Guermond, P. Minev, and J. Shen. An overview of projection methods for incompressible flows. *Computer methods in applied mechanics and engineering*, 195(44-47):6011–6045, 2006.
[23] A. C. Guyton and J. E. Hall. *Textbook of Medical Physiology*. Elsevier Saunder, 11 edition, 2006.
[24] J. G. Heywood and R. Rannacher. Finite-element approximations of the nonstationary Navier–Stokes problem. part IV: Error estimates for second-order time discretization. *SIAM J. Numer. Anal.*, 27(2):353–384, 1990.
[25] J. G. Heywood, R. Rannacher, and S. Turek. Artificial boundaries and flux and pressure conditions for the incompressible Navier–Stokes equations. *International Journal for Numerical Methods in Fluids*, 22(5):325–352, 1996.
[26] M. Ismail, A. Comerford, and W.A. Wall. Coupled and reduced dimensional modeling of respiratory mechanics during spontaneous breathing. *International Journal for Numerical Methods in Biomedical Engineering*, 29(11):1285–1305, 2013.
[27] M. Ismail, V. Gravemeier, A. Comerford, and W.A. Wall. A stable approach for coupling multidimensional cardiovascular and pulmonary networks based on a novel pressure-flow rate or pressure-only neumann boundary condition formulation. *International Journal for Numerical Methods in Biomedical Engineering*, in press, 2013.
[28] H. J. Kim, C. . Figueroa, T. J. R. Hughes, K. E. Jansen, and C. A. Taylor. Augmented Lagrangian method for constraining the shape of velocity profiles at outlet boundaries for three-dimensional finite element simulations of blood flow. *Computer Methods in Applied Mechanics and Engineering*, 198(45-46):3551–3566, 2009.
[29] C. Kleinstreuer, Z. Zhang, Z. Li, W. L. Roberts, and C. Rojas. A new methodology for targeting drug-aerosols in the human respiratory system. *International Journal of Heat and Mass Transfer*, 51(23-24):5578–5589, 2008.
[30] A. P. Kuprat, S. Kabilan, J. P. Carson, R. A. Corley, and D. R. Einstein. A bidirectional coupling procedure applied to multiscale respiratory modeling. *Journal of Computational Physics*, 244:148–167, 2013.
[31] B. Maury. *The respiratory system in equations*, volume 7 of *MS&A. Modeling, Simulation and Applications*. Springer-Verlag Italia, Milan, 2013.
[32] V. Maz'ya and J. Rossmann. L_p estimates of solutions to mixed boundary value problems for the Stokes system in polyhedral domains. *Math. Nachr.*, 280(7):751–793, 2007.
[33] V. Milišić and A. Quarteroni. Analysis of lumped parameter models for blood flow simulations and their relation with 1D models. *ESAIM: Mathematical Modelling and Numerical Analysis*, 38(4):613–632, 2004.
[34] J. M. Oakes, A. L. Marsden, C. Grandmont, S. C. Shadden, C. Darquenne, and I. E. Vignon-Clementel. Airflow and particle deposition simulations in health and emphysema: From in vivo to in silico animal experiments. *Annals of biomedical engineering*, pages 1–16, 2014.
[35] A. Porpora, P. Zunino, C. Vergara, and M. Piccinelli. Numerical treatment of boundary conditions to replace lateral branches in hemodynamics. *International Journal for Numerical Methods in Biomedical Engineering*, 28(12):1165–1183, 2012.
[36] A. Quarteroni, S. Ragni, and A. Veneziani. Coupling between lumped and distributed models for blood flow problems. *Computing and Visualization in Science*, 4(2):111–124, 2001. 10.1007/s007910100063.
[37] A. Quarteroni and A. Valli. *Numerical approximation of partial differential equations*. Springer, 2nd edition, 2008.
[38] A. Quarteroni and A. Veneziani. Analysis of a geometrical multiscale model based on the coupling of ODEs and PDEs for blood flow simulations. *Multiscale Modeling & Simulation. A SIAM Interdisciplinary Journal*, 1(2):173–195, 2003.
[39] R. Temam. Une méthode d'approximation de la solution des équations de Navier-Stokes. *Bulletin de la Société Mathématique de France*, 96:115–152, 1968.
[40] R. Temam. Sur l'approximation de la solution des équations de Navier–Stokes par la méthode des pas fractionnaires (II). *Archive for Rational Mechanics and Analysis*, 33(5):377–385, 1969.
[41] I. E. Vignon-Clementel, C. A. Figueroa, K. E. Jansen, and C. A. Taylor. Outflow boundary conditions for three-dimensional finite element modeling of blood flow and pressure in arteries. *Computer Methods in Applied Mechanics and Engineering*, 195(29-32):3776–3796, 2006.
[42] W. A. Wall, L. Wiechert, A. Comerford, and S. Rausch. Towards a comprehensive computational model for the respiratory system. *International Journal for Numerical Methods in Biomedical Engineering*, 26(7):807–827, 2010.
[43] E. R. Weibel. *Morphometry of the Human Lung*. Springer-Verlag, 1963.
[44] J. B. West. *Respiratory Physiology: The Essentials*. Lippincott Williams & Wilkins, 2008.

Université Paris-Sud, Laboratoire de Mathématiques d'Orsay (CNRS UMR 8628), 91405 Orsay cedex, France
E-mail address: justine.fouchet-incaux@math.u-psud.fr

INRIA Paris-Rocquencourt, Project-team REO, Building 16, BP 105, 78153 Le Chesnay cedex, France
E-mail address: celine.grandmont@inria.fr

Université Paris Descartes, MAP5 (CNRS UMR 8145), 45 rue des Saints-Pères, 75270 Paris cedex 06, France
E-mail address: sebastien.martin@parisdescartes.fr